UNIVERSITY OF CALIFORNIA,
IRVINE

Performance of Pt:TiO_2-B based Li-ion batteries

THESIS

submitted in partial satisfaction of the requirements
for the degree of

MASTER OF SCIENCE

in Materials Science and Engineering

by

Hongkui Zheng

Thesis Committee:
Professor Xiaoqing Pan, Chair
Associate Professor Daniel Mumm
Assistant Professor Iryna Zenyuk

2019

DEDICATION

To

my parents and friends

in recognition of their support and help

TABLE OF CONTENTS

LIST OF FIGURES

LIST OF TABLES

ACKNOWLEDGMENTS

I would like to express my deepest appreciation to my thesis advisor and committee chair, Professor Xiaoqing Pan, who has encouraged me to explore in the field of lithium-ion batteries and TEM (Transmission Electron Microscopy), which will also be the major topic of my future PhD research. Without Prof. Pan's support and encouragement on this research project, this thesis would have not been possible. I would also like to express my appreciation to Associate Professor Daniel Mumm and Assistant Professor Iryna Zenyuk for being me thesis committee and providing insightful suggestions on my thesis research.

During the one-year study at Pan group, I have met so many helpful friends and colleagues that help me finish the master thesis successfully. Thanks for Dr. Kui Zhang and Dr. Sung Joo Kim's initial proposal and previous work on this project at Michigan University. I am also grateful for the help from Komal Syed and Tom Lee on obtaining and analyzing the electrochemical data. As for the TEM part of the project, I would like to express my thanks to Huaixun Huyan, Dr. Linze Li and Dr. Mingjie Xu for instructing me on the sample preparation and TEM operation at UC Irvine Materials Research Institute and Prof. Peng Wang and his students for TEM training at Nanjing University. I am grateful to Assistant Professor Wenpei Gao's help on my thesis and recommendation on my PhD application. Additional thanks to Dr. Xingxu Yan, Dr. Sheng Dai, Fan ye, Lei Su and Tongtong Huang for providing helpful advices on this project. I also appreciate all the students and people in Pan group, including Chris Addiego, Chaitanya Gadre and Peter Thieu, who encouraged me and helped me throughout my thesis research project.

In the end, I would like to express my deepest thanks to my parents for their unconditional love and support on my graduate study at the University of California, Irvine, which encourages me to push the limit of myself and explore further in the field of materials.

ABSTRACT OF THE THESIS

Performance of Pt:TiO_2-B based Li-ion batteries

By

Hongkui Zheng

Master of Science in Materials Science and Engineering

University of California, Irvine, 2019

Professor Xiaoqing Pan, Chair

In this master thesis research project, we synthesized the Pt:TiO_2-B thin films as the anode material for lithium-ion batteries using the pulsed laser deposition (PLD) method, which is a totally waterless process. Considering the poor electronic conductivity of TiO_2-B, we aim to upgrade the electrochemical performance of TiO_2-B by integrating Pt into its matrix to improve its electronic and ionic conductivity. By varying the oxygen partial pressure during the PLD synthesis, we obtained the Pt:TiO_2-B thin film with different Pt content of 1.5%, 6% and 12% revealed by Rutherford backscattering spectrometry (RBS) analysis. Materials characterization techniques, including XRD and TEM, were used to verify thin films' composition and structure. The as-prepared Pt:TiO_2-B thin films were then used to assemble full cells of lithium-ion batteries (LIBs) and examined by chronopotentiometry and cyclic voltammetry tests. The result indicates that Pt:TiO_2-B thin films present excellent electrochemical performance with high rate capacity and cycling stability, which reveals its promising application as anode materials for LIBs, and Pt dopant plays an important role in upgrading the TiO_2-B electrochemical performance. This project suggests

using PLD to synthesize TiO_2 based materials doped with conductive substances to improve its electrochemical conductivity is an effective and simple way to obtain high-performance anode materials for lithium-ion batteries.

CHAPTER 1: Introduction

1.1 Introduction to Lithium-ion Batteries

Energy, materials, and information technology are the three pillars of contemporary science. Energy has always played an important role in human life. In recent years, with the development of world economics, people's demand for energy storage materials has expanded tremendously. Battery can store electrical energy and provide electrical energy to other devices through energy conversion, which greatly mitigates the restriction of energy storage and conversion raised by climate and regional restrictions. Among them, lithium-ion batteries (LIBs) are now considered to be one of the most promising power sources for hybrid electric vehicles and electronic devices due to their high ratio capacity and high cycle stability. [1][2]

In 1976, M.S. Whittingham made the first lithium-ion battery using the Li-TiS_2 system. [3] However, it has not been successfully commercialized due to the serious safety hazards caused by lithium's dendrites. In 1980, Armond first proposed the idea of replacing the metal lithium as anode material in the lithium battery with insertion-compound.[4] In this new system, both the cathode and anode materials are capable of conducting the Li-ion intercalation/deintercalation, which help resolve the safety problems of lithium ion batteries. In the meantime, Li-insertion compounds ($LiMO_2$, M=Mn, Co, Ni) were synthesized successfully by Goodenough, [5] and found that lithium ions in Li-insertion compounds can reversibly intercalate and deintercalate. Auborn JJ successfully assembled the MoO_2 (WO_2) / $LiPF_6$-PC/$LiCoO_2$ rocking chair battery with good cycle stability in 1987, which proves that Armond's new system is feasible. [6] In 1990, SONY Corporation developed a lithium-ion battery using $LiCoO_2$/graphite, which overcomes the shortcomings of low cycle life and poor safety of LIBs.[7] It marks a significant breakthrough in the battery industry that lithium-ion batteries are commercially available.

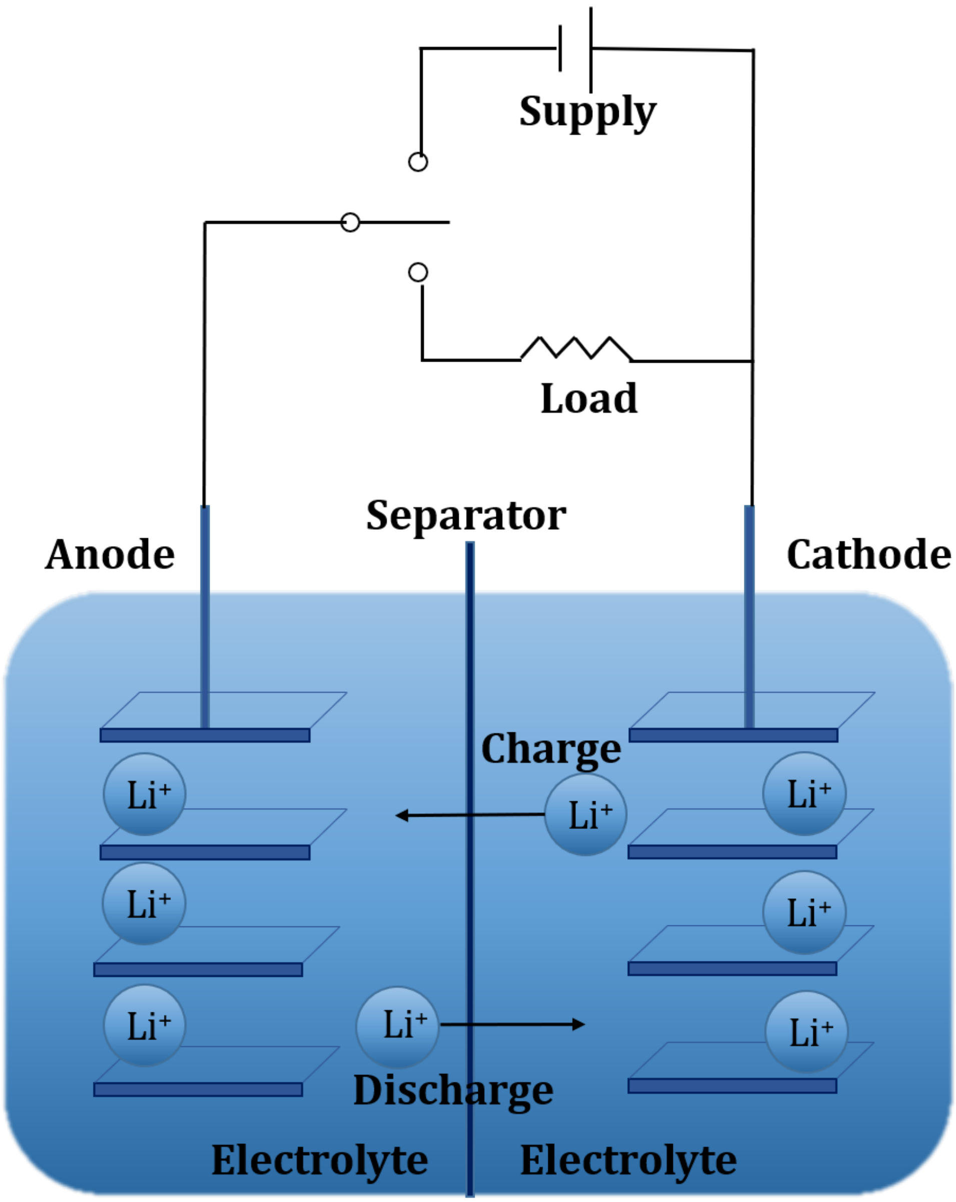

Figure 1.1 Schematic representation of rechargeable lithium-ion battery

Lithium-ion batteries consists of four parts as shown in Figure 1.1, including cathode, anode, electrolyte and separator. Layered substances that can store and exchange lithium ions easily and quickly are generally used as lithium-ion batteries' electrode materials.

Electrolyte, such as $LiPF_6$ and $LiClO_4$, plays an important role in transporting ions in lithium-ion batteries, while the main function of the separator, like glass fiber, polypropylene (PP) and polyethylene (PE), is to isolate the cathode and anode materials, so that the electrons in the lithium ion battery cannot transmit to form the short circuit, but the lithium ions in the electrolyte can pass freely.

The essence of lithium-ion battery is the difference of lithium ion's concentration in the system. During the charge process, lithium ions are extracted from cathode materials, diffused to anode through the electrolyte, and then embedded in the anode material's lattice to store energy. While the lithium ions are enriched near the anode, the cathode is in a lean lithium state, so electrons are transmitted to the anode through external circuit to make the charge in an equilibrium state. Discharge is just the opposite process. Lithium ions are released from the anode material, diffused to cathode through the electrolyte, and then embedded back to the cathode material's lattice to release energy. Thanks to the stable structure of the electrode materials, the intercalation/deintercalation process of lithium ions in the electrode materials will not damage its crystal structure but only cause a small change in the interlayer spacing, which ensures the reversibility of charge and discharge process and the stability of Li-ion batteries. During the charge and discharge process, lithium ions shuttle between the anode and the cathode and move like a rocking chair, which makes Li-ion battery also referred to as "Rocking chair battery".[4]

1.2 Cathode materials of Lithium-ion Batteries

Since cathode materials is the original source of lithium ions in the battery, it plays a significant role in the system of LIBs. Li-insertion compound, such as $LiCoO_2$, $LiMn_2O_4$ and

$LiFePO_4$, which can allow fast and reversible intercalation and deintercalation of Li-ions, are typically used as cathode materials.

The most commonly used cathode material is $LiCoO_2$.[9] With practical capacity of about 140 mAh/g, only half of the capacity of graphite as anode materials, LiCoO2 has been studied extensively by doping and coating to enhance its electrochemical performance. Higher capacity of the cathode or the anode will result in higher capacity of LIBs. In addition, cobalt is rare and very expensive, so it will greatly increase the cost of production of LIBs, which is not commercially favorable for the application of LIBs. Researchers dedicate to synthesize Li-insertion compound with lower content of cobalt and nickel and higher content of other easily available transition metals to lower the cost of cathode materials. High-performance cathode material that can be put into practical use is still being researched and developed.

1.3 Anode materials of Lithium-ion Batteries

Anode material is another core factor that matters the performance of LIBs. Three kinds of mechanism exist for anode material's role in LIBs. [11]

1) Intercalation materials, which have relatively low practical capacity but good cycling stability, including graphite, TiO_2 based materials and carbon-based materials, that have channels or layered space to accommodate Li-ion's intercalation and deintercalation.
2) Alloy materials, like Si and SnO_2 that have large specific capacity but poor cycling life because of the large volume expansion and distraction in the process of Li-ion's alloying and dealloying.

3) Conversion materials, such as transition metal oxides (Fe_2O_3, MnO_2, CuO), sulphides, nitrides and phosphides with large theoretical capacity but poor cycling performance due to the poor electrical conductivity and unexpected side reactions. These materials will react with Li-ions to form lithium compounds during the charge process.

Graphite is currently the mainstream commercial anode material of LIBs in electronic devices and electric vehicles. [12][13] However, practical application of LIBs has been greatly limited owing to the use of graphite anodes. [2] Its specific capacity has reached the limit and cannot meet the continuous large-current discharge capability required for large-scale power batteries which will lead to safety issues. [14] Research on viable methods to synthesize alternate anode materials with higher reversible capacity and cycling stability still needs to be carry out.

1.4 Introduction to TiO_2-B

Titanium dioxide (TiO_2) is a wide-used semiconductor material in many different applications. Developing anode material with good performance upon cycling is crucial for improving LIBs' performance, researchers have dedicated to studying TiO_2 as anode material because of its low cost, small volume change, environmental benignancy, high reversible specific capacity and chemical stability. [15][16][17][18] Moreover, TiO_2 has relatively high working voltage, so that the battery can effectively inhibit the formation of the solid electrolyte interphase (SEI) on the anode surface during the charging and discharging process, thereby improving the safety performance of the battery. There exist eight different kinds of TiO_2 crystals, [19][20][21][22][23][24] some of which are extensively used for LIBs' research, such as rutile and anatase. The mechanism of lithium ion' s insertion and extraction process in TiO_2 is shown below.

$$xLi^{+}+TiO_2+xe^{-} \rightleftharpoons Li_xTiO_2$$

Phase	Space group	Density(g/cm³)	Lattice parameters(Å)
Anatase	$I4_1/amd$	3.79	a=3.78, c=9.51
Rutile	$P4_2/mnm$	4.13	a=4.59, c=2.96
Brookite	Pbca	3.99	a=9.17, b=5.46, c=5.14
TiO_2-B	C2/m	3.62	a=12.18, b=3.74, c=6.52, β=107.05°
TiO_2-Ⅱ	Pbcn	4.33	a=4.52, b=5.5, c=4.94
TiO2-Ⅲ	$P2_1/c$	3.79	a=4.64, b=4.76, c=4.81, β=99.2°
TiO2-H	I4/m	3.46	a=10.18, c=2.97
TiO2-R	Pbnm	3.87	a=4.9, b=9.46, c=2.96

Table 1.1 Structure parameters of eight kinds of TiO_2 polymorphs

Among all the TiO_2 polymorphs, the bronze polymorph of titanium dioxide (TiO_2-B) is an excellent option for anode materials of LIBs because of its open structure and channel which are conducive to fast insertion and extraction process of lithium ions by a pseudocapacitive Faradaic process. [25][26][27] It was first synthesized by Marchand using hydrothermal method in 1980. [22] TiO_2-B's crystal structure belongs to monoclinic crystal system; the crystal structure of TiO_2-B is shown in the upper row of Figure 1.2. It is composed of TiO_6 octahedra that share edges and corners, and possesses open channels along the b-axis, which is favorable for the lithium-ion's intercalation and deintercalation process.

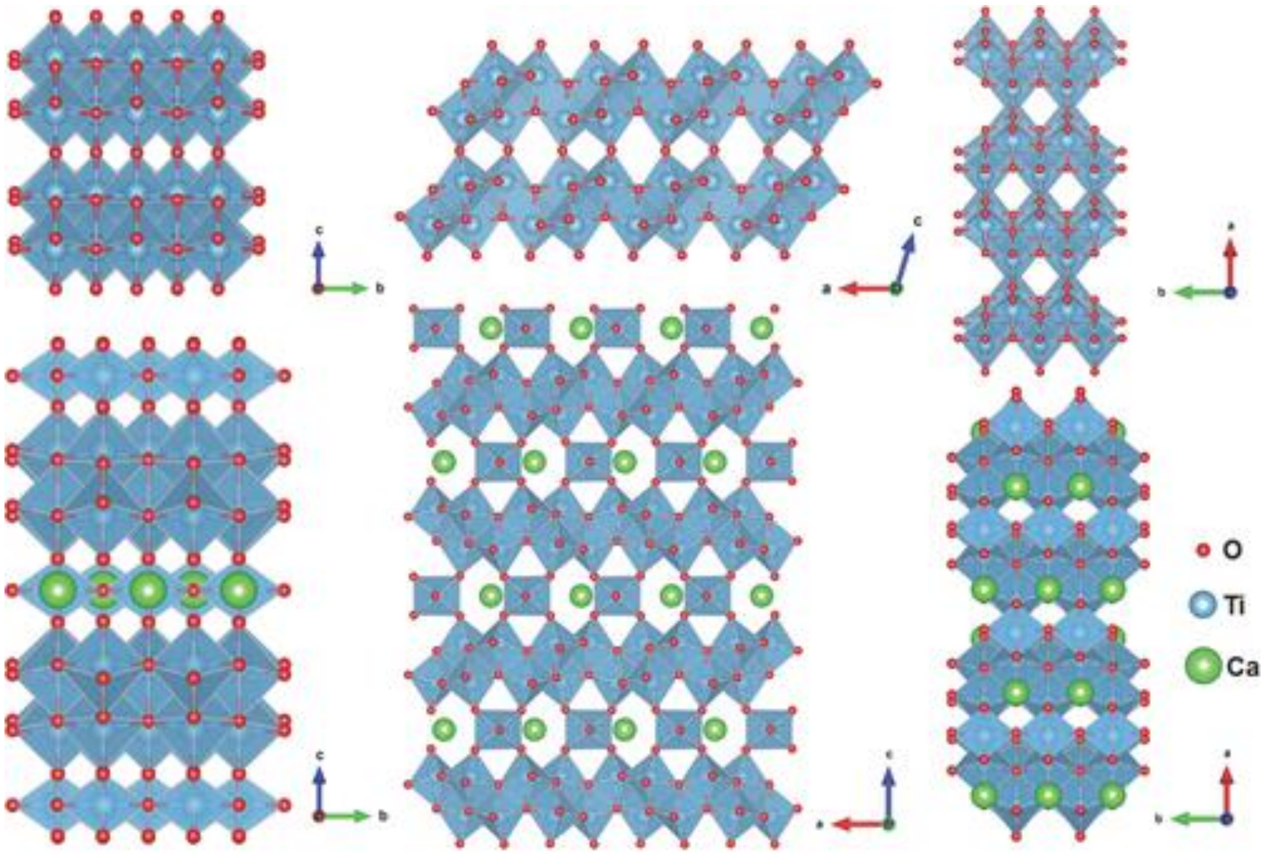

Figure 1.2 Crystal structure of TiO_2-B and Ca:TiO_2-B

Upper row: Crystal structure of TiO_2-B projected along: (a) [100] direction; (b) [010] direction; (c) [001] direction; Lower row: Crystal structure of Ca:TiO_2-B projected along: (a) [100] direction; (b) [010] direction; (c) [001] direction. [25]

$CaTi_5O_{11}$ (Ca:TiO_2-B) is a template layer used to stabilize TiO_2-B since Ca could stabilize the structure of TiO_2-B so that TiO_2-B could be deposited stably on $SrTiO_3$ substrate. Anatase phase, rather than TiO_2-B, will be obtained if we directly deposit pure TiO_2 on $SrTiO_3$ substrate, [28] but highly crystalline TiO_2-B will form on the a-b plane of $CaTi_5O_{11}$ layer by depositing pure TiO_2 on the $CaTi_5O_{11}$ layer above the $SrTiO_3$ layer, due to the closely related lattice structure between Ca:TiO_2-B and TiO_2-B phases. [25] The crystal structure of Ca:TiO_2-B is shown in the lower row of Figure 1.2, which is a variant phase of TiO_2-B structure with additional Ca atoms and superlattice twinning in essence. It belongs to orthorhombic crystal system and has lattice parameters of a=12.1702 Å, b=3.8012 Å, c=17.9841 Å. Open channels along b-axis are also visible in the Ca:TiO_2 structure. Thus, it will be conducive to the transport of Li-ions during the charge and discharge process. However, as a semiconductor material, TiO_2-B has low electronic and ionic conductivity and has relatively low theoretical capacity, which limits its application as a potential high-performance anode material. Researchers have tried to incorporate TiO_2-B with conductive materials, such as carbon nanotubes(CNTs) and reduced graphite oxide(RGO), to improve electronic conductivity and accelerate the lithium ion transmission speed, thus to enhance the electrochemical performance of TiO_2-B. [29][30][31][32][33] Nevertheless, TiO_2 on the CNTs and RGO surface will still subject to the huge volume change and decomposition during the charging and discharging process, which results in the degradation of electrode materials as cycling. [34] Another way to promote the performance of TiO_2 is to use nanocrystalline TiO_2 as anode materials. [35][36] When material size is reduced to the nanometer level, it can effectively shorten the diffusion distance of lithium ions and electrons, increase the specific contact area between the electrolyte and the electrode. Therefore, it can improve the electrochemical performance of TiO_2. In recent years, TiO_2 has been extensively studied in various forms, such as nanotubes, nanowires, nanoparticles and nanosheets. [37][38][39][40] The challenge is that such measures can only change the electrical conductivity between the surface of the electrode and adjacent ions, but the intrinsic resistance of TiO_2 is not effectively improved.

1.5 Objective and Outline of this thesis

Herein, we intend to upgrade the electrochemical performance of TiO_2-B by doping Pt inside TiO_2-B matrix[41]. In this project, we change the Pt content in TiO_2-B thin films by varying the oxygen partial pressure in order to find the most suitable preparation environment of Pt:TiO_2-B, and hence to better the electrochemical performance of Pt:TiO_2-B. Crucially, we prepare TiO_2-B with a waterless process[25] rather than hydrothermal methods which is typically used [40][42][43][44][45][46][47], but it will introduce water into the TiO_2-B lattice structure which will result in the randomized crystal orientation and impurity of TiO_2-B lattice [48]. Thus, we can dope the pure TiO_2-B with Pt, which lay a solid foundation for its application in LIBs. Using epitaxial crystalline TiO_2-B films, grown by pulsed laser deposition (PLD), it shows that by increasing the oxygen partial pressure in pulsed laser deposition, Pt content decreased in TiO_2-B films. Our results show that Pt:TiO_2-B thin films present excellent electrochemical performance with high rate capacity and cycling stability, which reveals its promising application as anode materials for LIBs.

This thesis consists of the following chapters:

CHAPTER 1: Introduction

CHAPTER 2: Synthesis and characterization of Pt:TiO_2-B thin film

CHAPTER 3: Results and discussion

CHAPTER 4: Conclusions and future work

CHAPTER 2: Synthesis and characterization of Pt:TiO_2-B thin film

2.1 Introduction

In this chapter, methods and experimental procedures of synthesis and characterization of Pt:TiO_2-B thin film are discussed. Pulsed laser deposition (PLD), a totally waterless process, is used to deposit Ca:TiO_2-B and Pt:TiO_2-B on (100) $SrTiO_3$ substrate. Rutherford backscattering spectrometry (RBS), Hall measurement, X-ray diffraction (XRD) and Transmission electron microscopy (TEM) are tested for analysis of chemical composition and structural characterization of the as-prepared Pt:TiO_2-B thin film. Chronopotentiometry and Cyclic Voltammetry (CV) tests are carried out to test the electrochemical performance of Pt:TiO_2-B as anode material of Lithium ion batteries.

2.2 Epitaxial growth by pulsed laser deposition (PLD)

Epitaxial growth refers to the deposition of a crystalline overlayer on a crystalline substrate with the same crystal orientation. Ca:TiO_2 and Pt:TiO_2 thin films used in this thesis were prepared in the same way as our group's previous experiments[25][41]. The $CaTi_4O_9$ sample applied to grow Ca:TiO_2-B thin films were prepared by blending 80% TiO_2 and 20% CaO powders, sintering at 1400℃, and pressed into a pellet under the force of 10000lb. The Pt:TiO_2 sample used for Pt:TiO_2-B thin film growth was prepared by mixing 50% of TiO_2 and 50% PtO_2 powder and treated in the same way as preparing $CaTi_4O_9$ sample. At a repetition rate of 10Hz, a 248-nm KrF excimer laser with a pulse duration of 22ns and a fluence of ~3.4J·cm^{-2} was used for pulse laser deposition under a base pressure of <10^{-7} Torr. Ca:TiO_2-B thin film was deposited on a (100) $SrTiO_3$ substrate at 800℃ in the oxygen ambient of 0.05Torr for an hour, while the Pt:TiO_2-B thin film was deposited on the same substrate at 550℃ in the oxygen ambient of 6mTorr, 16mTorr, 50mTorr for an hour, respectively, which corresponds to 12%, 6%, 1.5% of Pt content in each Pt:TiO_2 sample, respectively. Results are revealed by Rutherford backscattering spectrometry (RBS) analysis[41].

2.3 Composition and Structural characterization

Rutherford Backscattering Spectrometry (RBS) was conducted in a Tandetron high voltage particle accelerator at Michigan Ion Beam Laboratory. TiO_2-B and Pt:TiO_2-B samples are all cut into 6*6mm pieces. From a deuterium source, A 30° beamline was energized at 1MeV under room temperature. The experimental spectra were fitted using the SIMNRA software to obtain elemental information; we set Pt, Ti, O compositions as the variable parameters in the software.

Hall effect measurement of Pt:TiO_2-B samples was conducted on MMRH-50 Hall and measurement system at Michigan University in the Vander Pauw configuration, [49] which aims to measure the electrical properties of Pt:TiO_2-B thin films. Formulas to calculate the resistivity (ρ), carrier concentration (n) and Hall mobility (μ) are shown below.

$$\rho = R_S d = \frac{\pi d}{\ln 2}\frac{\overline{V_{ij}}}{I_{kl}} f \qquad (i, j, k, l = 1,2,3,4)$$

$$n = \frac{n_S}{d} = \frac{8\times10^{-8} IB}{ed}\frac{1}{\sum\left(V_{ij}^{+B} - V_{ij}^{-B}\right)}$$

$$\mu = \frac{1}{e\rho n}$$

R_s is the sheet resistance, d is the film thickness, f is the sample geometry factor, which takes the value between 0-1, n_s is the sheet carrier density and e is the elementary charge. The X-ray diffraction(XRD) patterns were obtained on a Rigaku rotating-anode diffractometer and Rigaku smart-lab X-ray diffractometer using the parallel beam optics within 2θ range from 7° to 80°. The X-ray generator was operated at 40kV and 44mA using Cu Kα radiation (λ = 0.15406 nm). Films' thicknesses were measured by a Veeco Dektak profilometer and confirmed with TEM images. The thickness value is used to calculate the mass of anode materials and specific capacity for electrochemical test. Using a JEOL JEM 2100F TEM and JEOL Grand Arm-300CF TEM equipped with a spherical aberration corrector (Cs-corrected) operated at 300kv, we observe the morphology and microstructure of the as-prepared Pt: TiO_2-B thin films. Cross-sectional TEM samples were prepared by using the Allied High Tech Multiprep system and Gatan PIPS (Precision ion polishing system), since well-prepared TEM specimens is the foundation for high quality TEM images.

2.4 Electrochemical test

Electrochemical tests aim to understand the process of Li-ion's intercalation and deintercalation in the electrode, which relates to the electrochemical performance of electrode materials. To find out the electrochemical performance of Pt:TiO_2-B thin film as anode materials, thin films were assembled in full cells, in which metallic Li acts as counter and reference electrode. Battery cells were assembled in a glove box filled with argon, with O_2 and H_2O levels below 2 and 1 ppm, respectively. The assembly schematic diagram of test cells is shown in Figure 2.1. Electrochemical experiments were tested at room temperature on a Princeton Applied Research VersaSTAT MC 4-channel system operating in the galvanostatic mode using lithium metal anode, non-aqueous electrolyte (1mol $LiPF_6$ in ethylene carbonate: dimethyl carbonate 1:1(v/v), Sigma-Aldrich) and an l.55mm-thick glass fiber separator between two electrodes. The structure of EL-Cell ECC-Std electrochemical cell and Princeton Applied Research VersaSTAT multichannel electrochemical testing system are shown in Figure 2.2 and 2.3. The potentiostat possesses five electrode lead, including working electrode (WE, electrode material of interest) lead, counter electrode (CE) lead, sense electrode (SE, usually connects to the working electrode, which combination often referred to as the working-sense) lead, reference electrode (RE, measures/controls the voltage between itself and the sense electrode) lead and ground lead. Batteries, capacitors and fuel cells are generally connected using the two-electrode connection as shown in Figure 2.4(a). Aqueous electrochemistry experiments and EIS experiments are usually connected using the three-electrode connection shown in Figure 2.4(b), while some specific experiments might require four-electrode connection as shown in Figure 2.4(c). All electrochemical experiments in this thesis adopt the two-electrode connection. Cycled cells were separated in the same glove box, and post-cycling films were washed in dimethyl carbonate (obtained from Sigma-Aldrich) three times and dried in the fume hood overnight before XRD and TEM tests.

The electrochemical experiment data of Ca:TiO_2-B and Pt:TiO_2-B thin films as anode material are all obtained on VersaStudio software and tested by the VersaSTAT system. Figure 2.5 and 2.6 show the screenshot of the VersaStudio software in Chronopotentiometry and Cyclic Voltammetry (CV) experiment on Pt:TiO_2-B thin film.

In order to conduct the chronopotentiometry experiment, the first step is to calculate the 1C current for the electrode material of interest. For the Ca:TiO_2-B sample, it has a theoretical density of 3.637 g cm^{-3} and a specific capacity of 294mA h/g, so a 160nm thick Ca:TiO_2-B thin film with the area of 0.243cm^2 has a theoretical capacity of:

$$160\times10^{-7}cm\times0.243cm^2\times3.637g/cm^3\times294mAh/g=4.16\times10^{-3}\ mAh$$

Since 1C refers to full charge or discharge its capacity in one hour, 1C current equals to 4.16uA for this sample. For Pt:TiO_2-B thin films, it is difficult to calculate the theoretical weight of each sample with Pt dopant. And to measure the actual mass by a balance is not applicable with the mass of several micrograms. Calculation on Pt:TiO_2-B thin films' chronopotentiometry experiments will be discussed later after obtain the RBS result of the chemical composition of targeted materials to calculate the sample weight so that 1C current of each sample could be calculated.

The battery capacity of each sample is calculated by multiplying the time period (h) with the current (mA); the specific capacity is obtained by dividing the battery capacity by the mass of each sample. The Coulombic efficiency of electrode materials for lithium ion batteries is defined as below.

Coulombic efficiency= lithium ions that can be extracted/ lithium ions that can be stored, which also equals to the value of discharge capacity over charge capacity. The higher the value of Coulombic efficiency is, the better the cycle stability of the electrode material will be, with more Li ions could be constantly extracted from the electrode material.

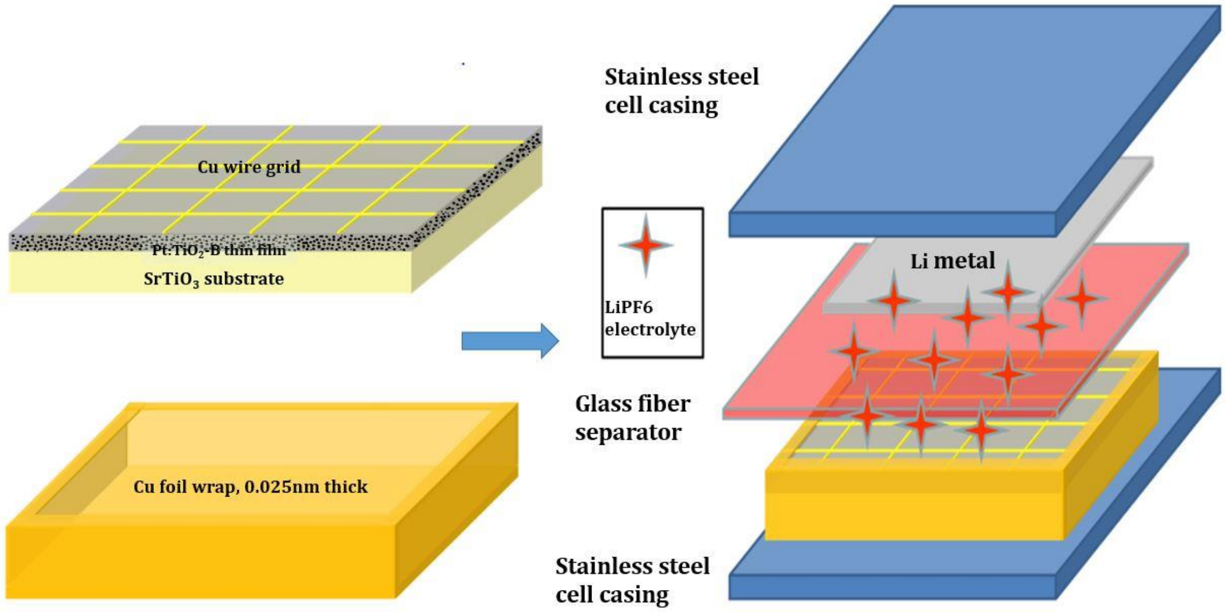

Figure 2.1 Assembly schematic diagram of test cells.

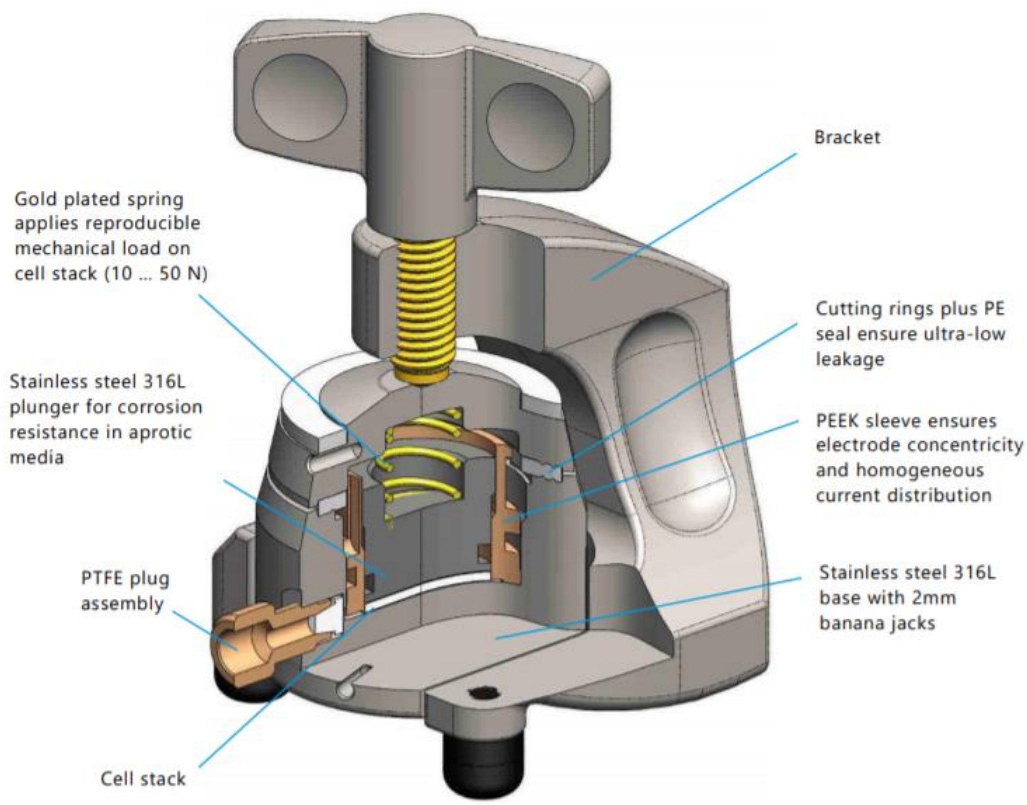

Figure 2.2 Structure of EL-Cell ECC-Std electrochemical cell. https://el-cell.com/

Figure 2.3 Princeton Applied Research VersaSTAT multichannel electrochemical testing system. https://www.ameteksi.com/

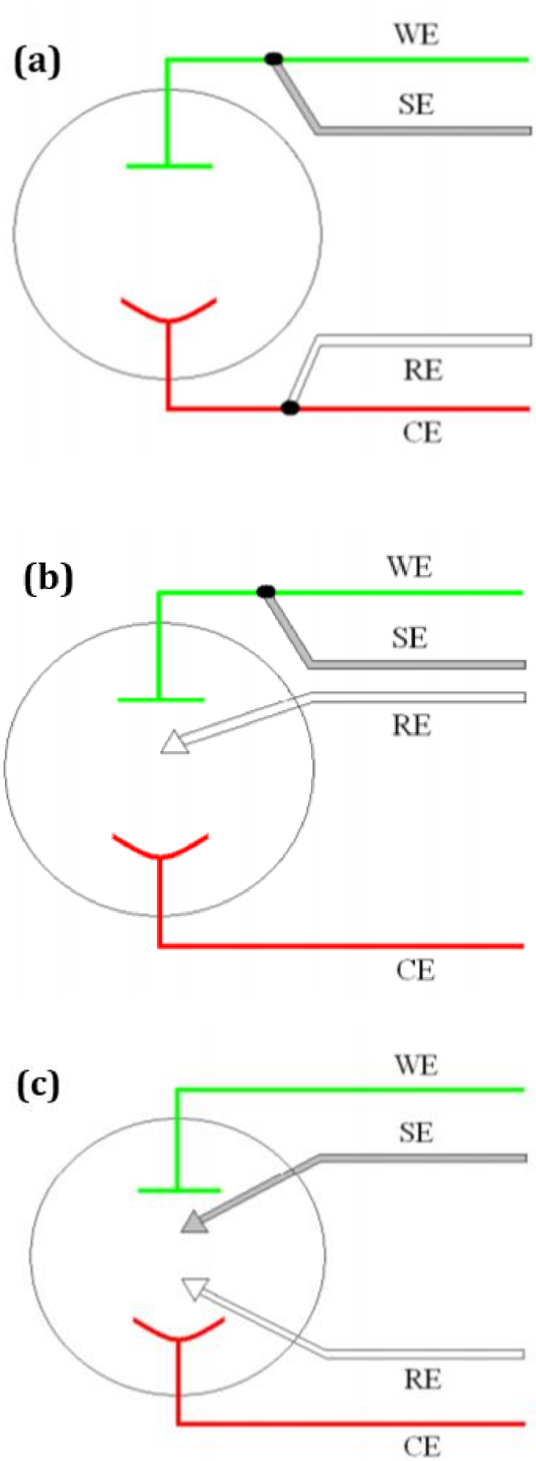

Figure 2.4 Three kinds of electrode connection (a)Two electrode connection; (b)Three electrode connection; (c)Four electrode connection. https://www.ameteksi.com/

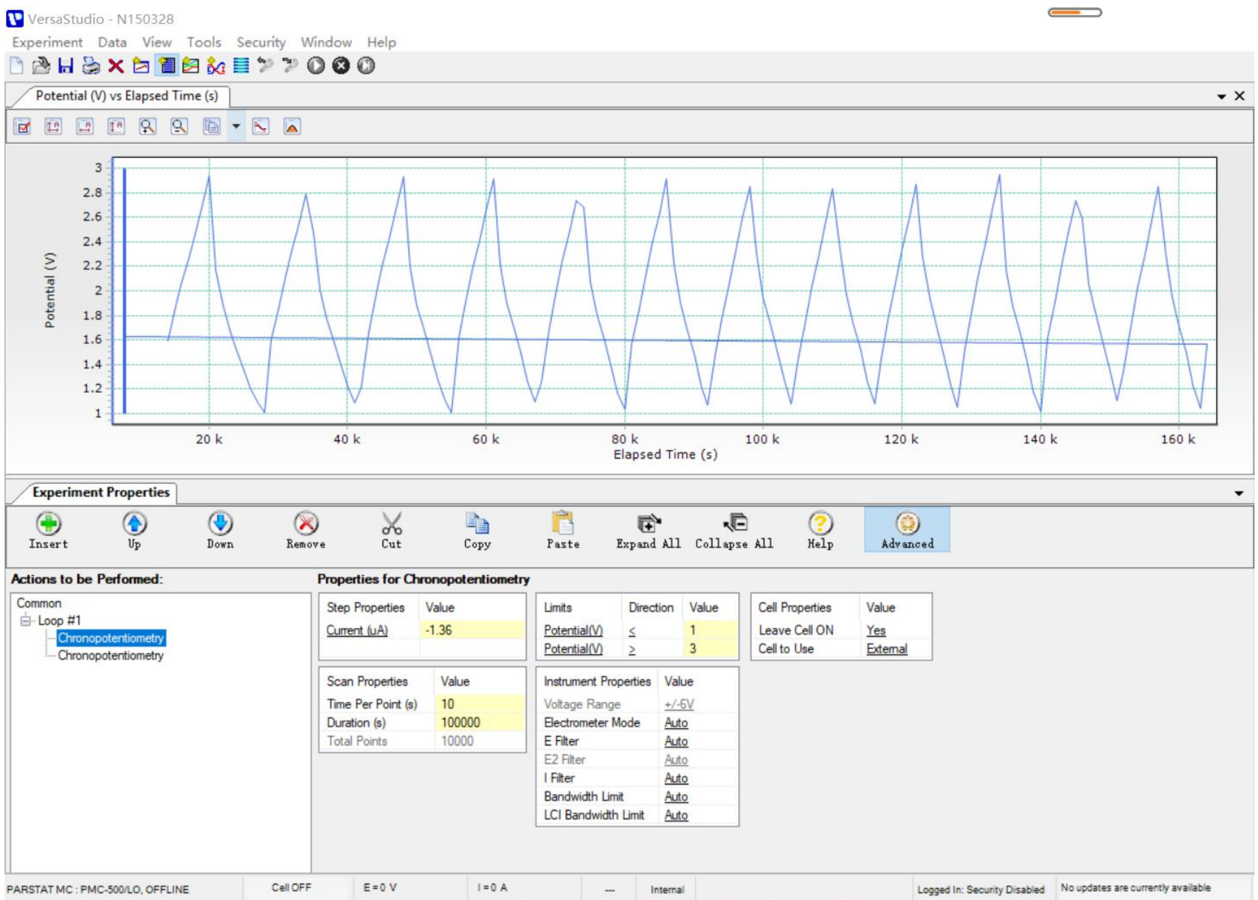

Figure 2.5 Screenshot of VersaStudio software in a chronopotentiometry experiment on Pt:TiO_2-B thin film. The 1C current is set as 1.36uA and the voltage range is 1-3V.

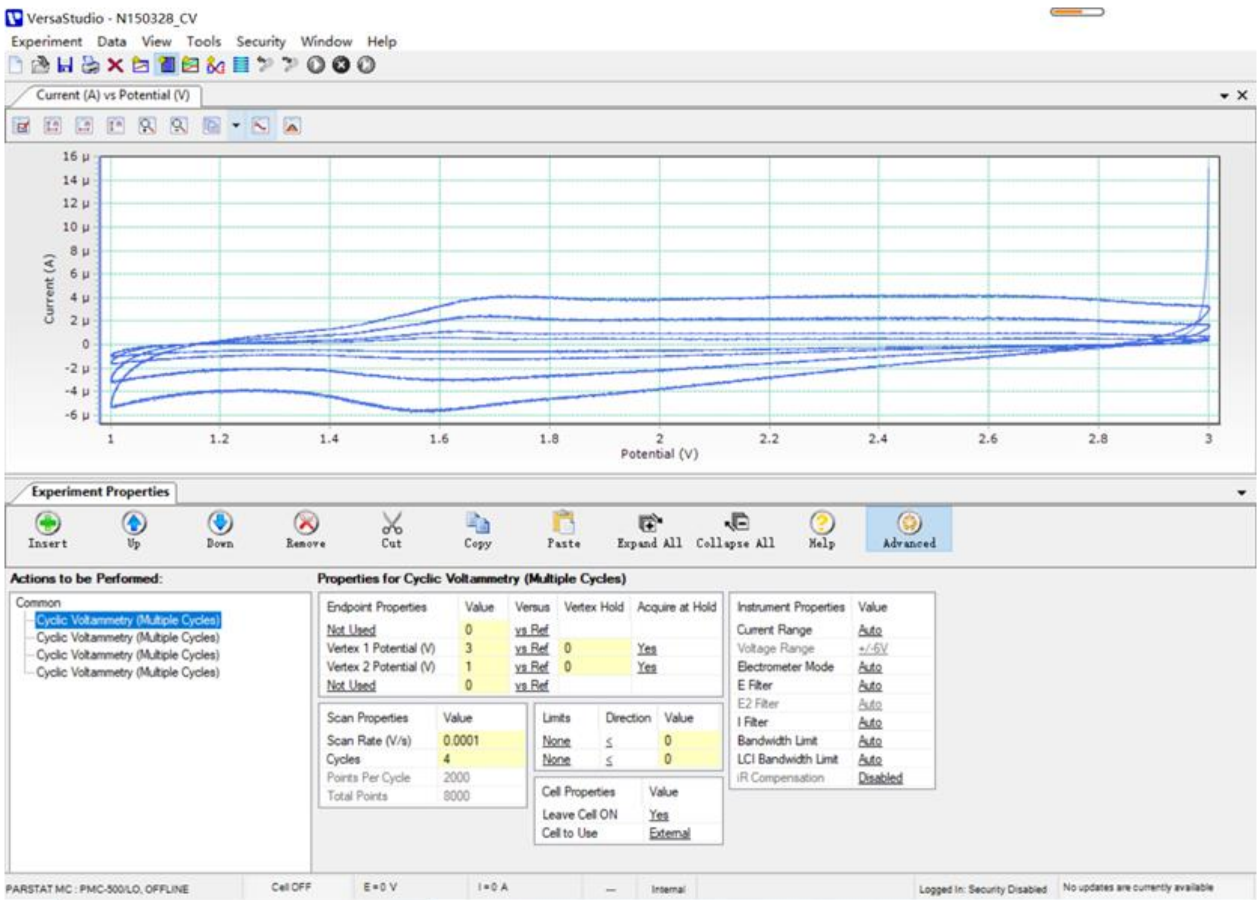

Figure 2.6 Screenshot of VersaStudio software in a Cyclic Voltammetry experiment on Pt:TiO_2-B thin film. The voltage range is 1-3V and the scan rate is 0.1mV/s.

CHAPTER 3: Results and discussion

3.1 Rutherford Backscattering Spectrometry (RBS)

$P(O_2)$ (mTorr)	Pt(at%)	Ti(at%)	O(at%)	X in TiO_x
6	12	30	58	1.9
30	6	33	61	1.8
50	1.5	33.5	65	1.9

Table 3.1 RBS analysis of the chemical composition of Pt:TiO_2 thin films versus $P(O_2)$ [41]

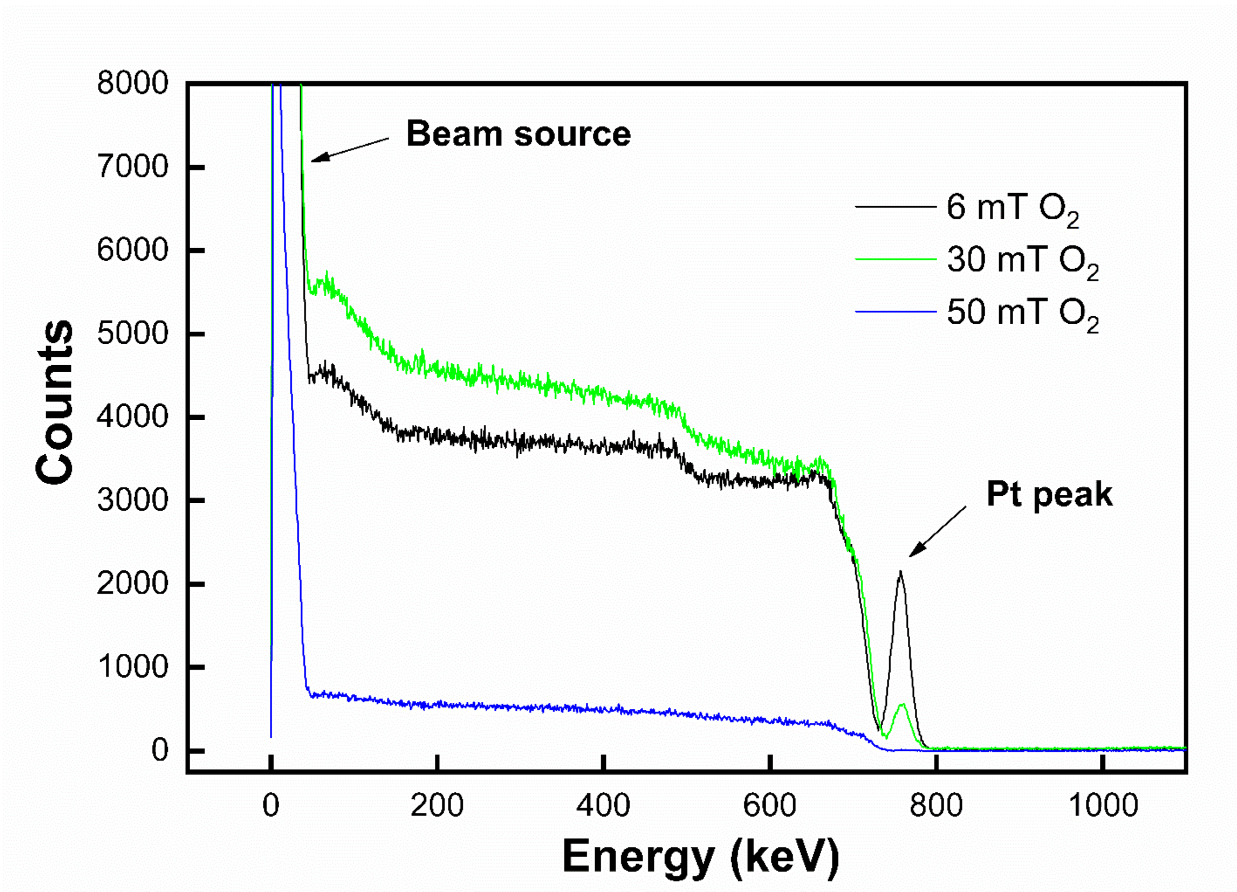

Figure 3.1 RBS result of Pt:TiO_2 thin films.

According to Rutherford Backscattering Spectrometry result in Table 3.1 and Figure 3.1, Pt peak can be clearly identified and we can easily find that with the increase of oxygen partial pressure in pulsed laser deposition, Pt content, which corresponds to the density of Pt:TiO_2 thin films, decreased in TiO_2-B films, so the Pt peak is more pronounced with lower oxygen partial pressure. This phenomena might result from the presence of oxygen vacancies, [50][51][52] these vacancies will perform as potential sites for the growth of Pt nanoparticles. [41][53][54] Thus, higher P(O_2) will result in lower Pt content in Pt:TiO_2-B thin films.

3.2 Hall effect measurement

	6mT O_2 Pt-TiO_2-B (12% Pt)	**30mT O_2 Pt-TiO_2-B** (6% Pt)	**50mT O_2 Pt-TiO_2-B** (1.5% Pt)
Film Thickness d (nm)	58.6	29.2	30
Carrier Conc. n (cm^{-3})	7.27×10^{13}	4.01×10^{9}	2.22×10^{9}
Resistivity **ρ ($\Omega\cdot$cm)**	1.40×10^{4}	6.29×10^{4}	1.16×10^{5}
Mobility **μ (cm^2/V$\cdot$s)**	6.13	-- too resistive	-- too resistive

Table 3.2 Hall effect measurement of Pt:TiO_2 thin films

The result of Hall effect measurement reveals that 12% Pt content can increase the conductivity of Pt:TiO_2 thin films, while 6% Pt content's enhancement on conductivity is not large enough to be measured. It should be noticed that these resistive thin films will bring unexpected experimental error when conducting the electrochemical test. Since both the $SrTiO_3$ substrate and the Pt:TiO_2 thin films are not conductive, copper foil warp has to be added when assembling the full cell to make the whole system works, which might influence the electrochemical performance of Pt:TiO_2 thin films.

3.3 X-Ray Diffraction (XRD)

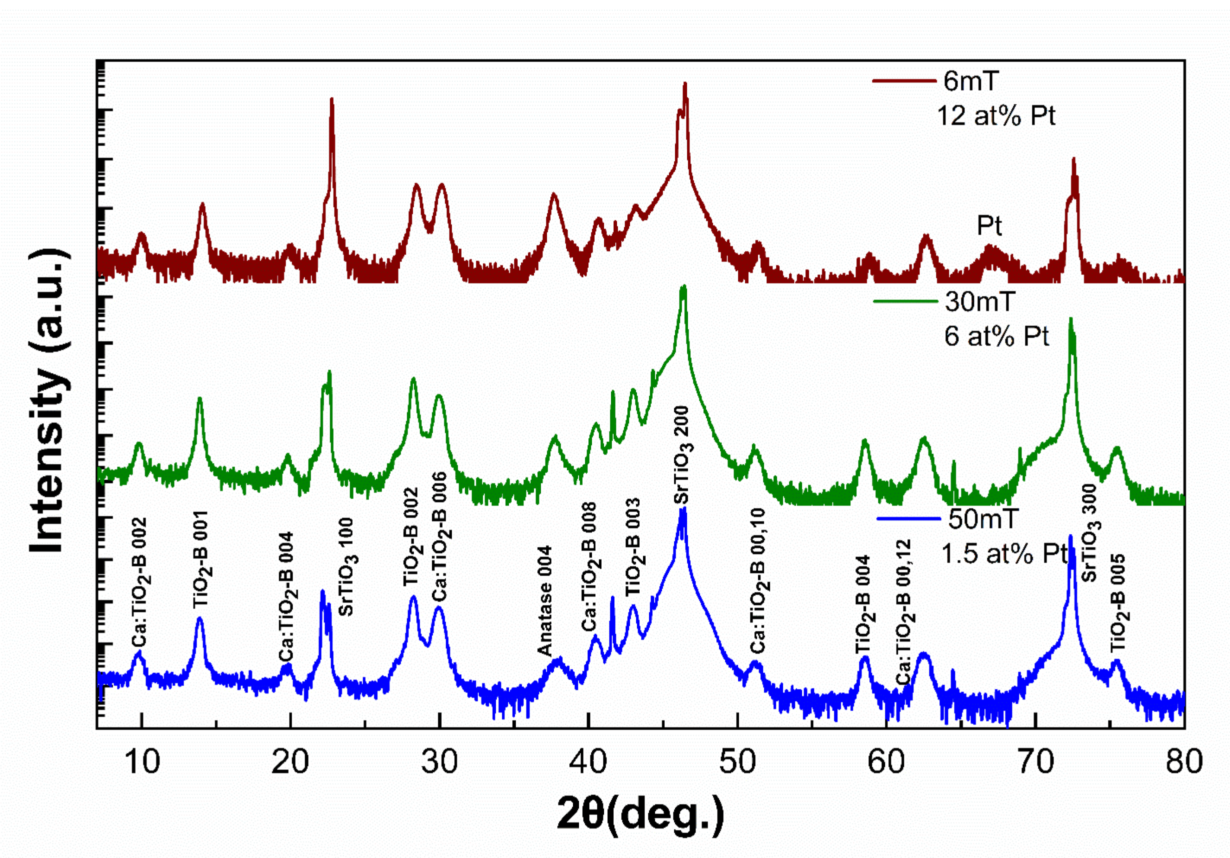

Figure 3.2 XRD pattern of as-prepared Pt:TiO_2-B thin films on (100) $SrTiO_3$ substrate with Pt content of 1.5%, 6% and 12%.

Figure 3.2 shows the θ−2θ X-ray diffraction (XRD) pattern of as-prepared Pt:TiO_2-B thin film with different Pt content. Ca:TiO_2-B, TiO_2-B and $SrTiO_3$ substrate can be clearly discerned in the XRD pattern, and Pt peak can also be identified in the Pt:TiO_2-B thin films with Pt content of 12%, but lower Pt content cannot be recognized in the XRD pattern due to the insufficient amount of Pt in the sample.

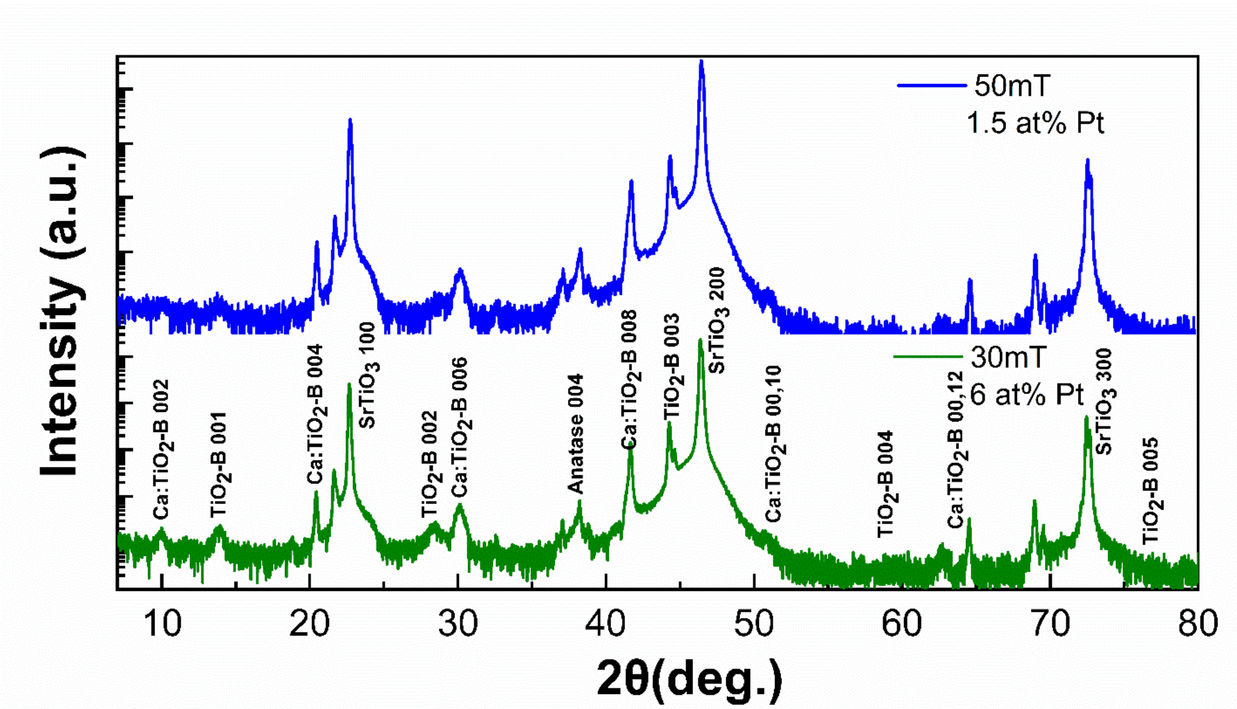

Figure 3.3 XRD pattern of post-cycling Pt:TiO_2-B thin films on (100) $SrTiO_3$ substrate with Pt content of 1.5% and 6%.

The potential anode materials' response to long cycling was examined by XRD to check if there are any changes of phases after intensive cycling. After cycling for thousands of times, compared with the XRD pattern of as-prepared Pt:TiO_2-B thin films, XRD pattern of post-cycling Pt:TiO_2-B thin films, as shown in Figure 3.3, are essentially unchanged, which indicates that most phases of Pt:TiO_2-B thin film are kept the same during the charge and discharge process. Thus, Pt:TiO_2-B thin film is stable as anode material for lithium-ion batteries.

3.4 Transmission Electron Microscopy (TEM)

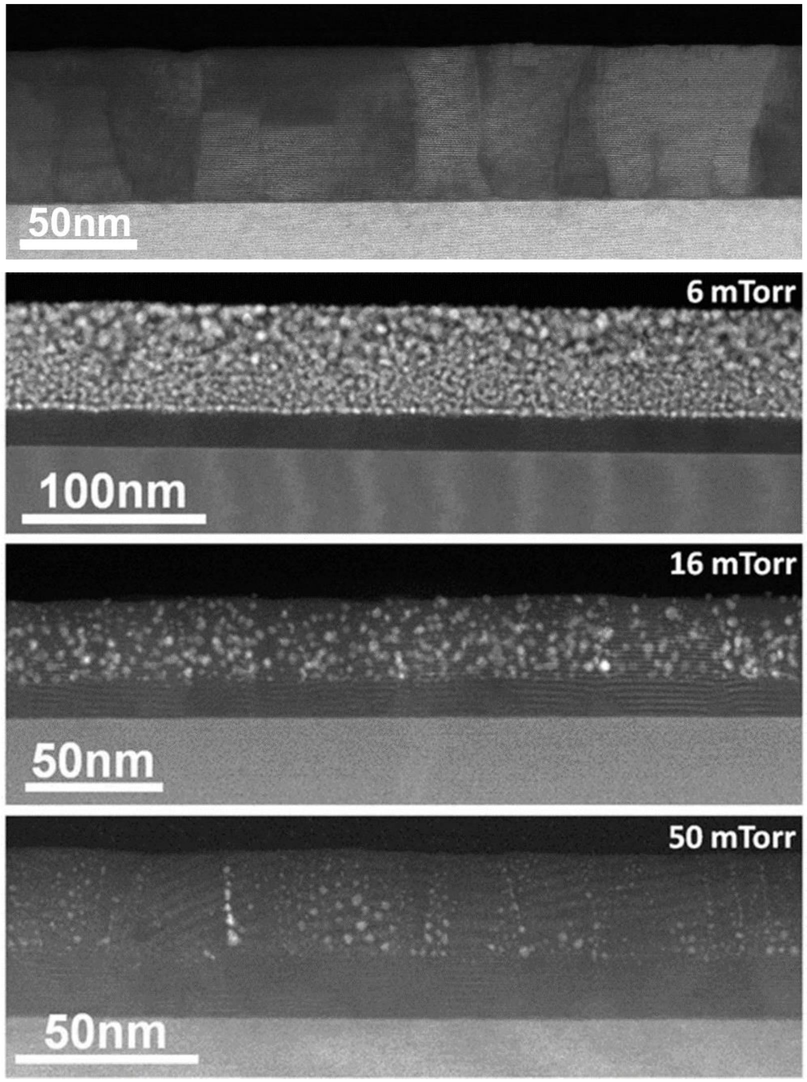

Figure 3.4 STEM-HAADF images of Ca:TiO_2-B and Pt:TiO_2-B thin films on (100) $SrTiO_3$ substrate grown under oxygen partial pressures of 6, 16 and 50 mTorr, which equals to Pt content of 12%, 6%, 1.5%, respectively. [41]

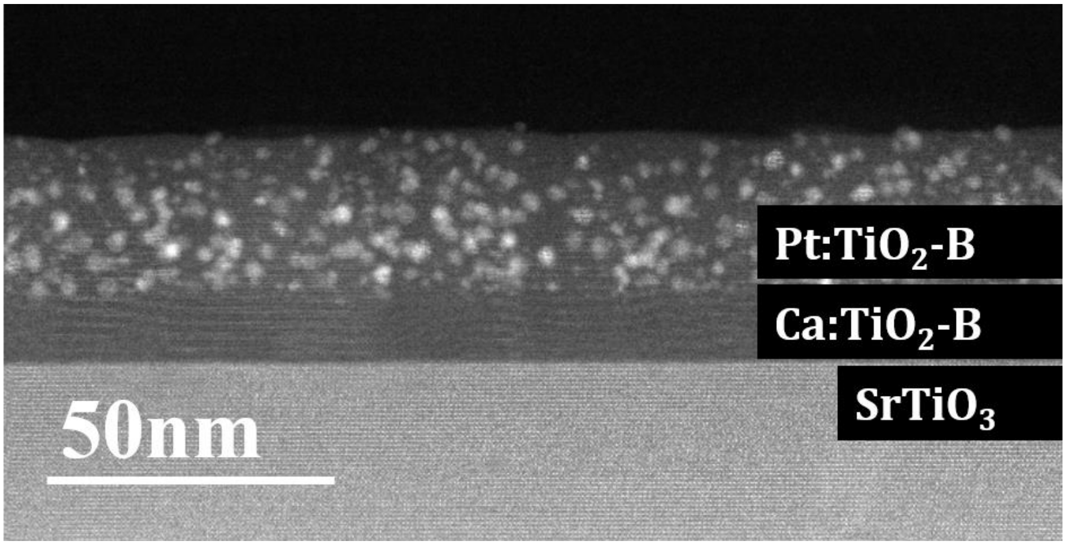

Figure 3.5 STEM-HAADF images of Pt:TiO_2-B thin film grown under 16mTorr on (100) SrTiO3 substrate templated with Ca:TiO_2-B.

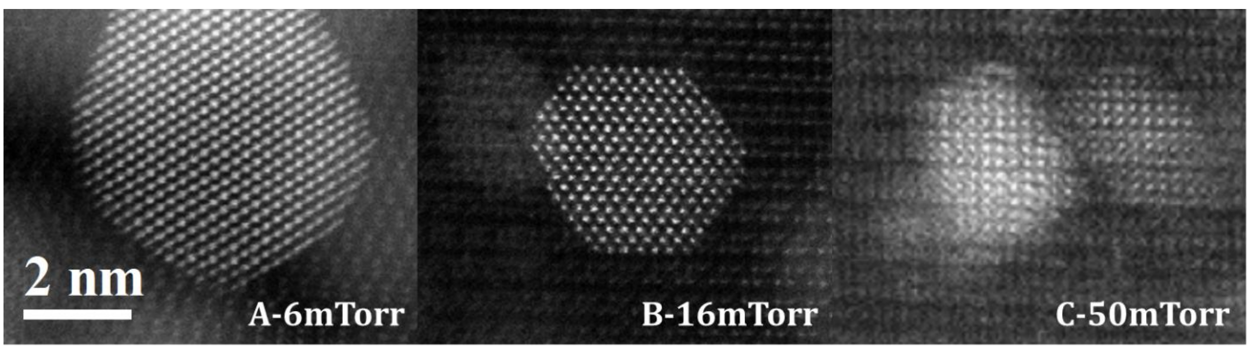

Figure 3.6 (A-C) High-resolution HAADF images of Pt nanoparticles under various oxygen partial pressures of 6, 16 and 50mTorr.

In order to change different Pt content in the Pt:TiO_2-B thin films, three different oxygen partial pressure-p(O_2), which was kept below 100mTorr to hinder the formation of Pt oxide, was used for Pt:TiO_2-B thin films growth. An overview image of as-prepared Ca:TiO2-B and Pt:TiO_2-B thin films on (100) $SrTiO_3$ substrate under different oxygen partial pressure is shown in Figure 3.4. From the STEM-HAADF (Scanning Transmission Electron

Microscopy-High-Angle Annular Dark Field) image, with the increase of oxygen partial pressure in pulsed laser deposition, Pt's distribution become more scarce in Pt:TiO_2-B thin films. We can clearly see the layered structure of Pt:TiO_2-B thin film on (100) SrTiO3 substrate templated with Ca:TiO_2-B in Figure 3.5 and the layer thickness of Pt:TiO_2-B can also be verified in the STEM image. From the high-resolution HAADF images of Pt nanoparticles in Figure 3.6, Pt nanoparticles' crystallographic change raised by different oxygen partial pressure can also be identified.

3.5 Chronopotentiometry tests

For the C-rate currents used for chronopotentiometry tests of Pt:TiO_2-B thin films were calculated based on theoretical capacity of TiO_2-B of 335 mA h/g. and theoretical density of 3.616g/cm^3, and platinum's theoretical density is 21.45 g/cm^3.

According to the RBS result, the Pt:TiO_2-B thin film with Pt content of 1.5% has 33.5% Ti and 65% O. The mass of the sample is $4.06*10^{-6}$g as calculated as below.

The sample's area is 0.278 cm^2 and it has the thickness of 30nm, so the sample's volume is $8.35*10^{-6}cm^3$.

V%=atomic weight% / density

$V_{TiO2\text{-}B}\%=(0.335*47.87g/mol+0.65*16g/mol)/3.616g/cm^3=7.311$

$V_{Pt\%}=0.06*195.078/21.45=0.546$

$V_{TiO2\text{-}B}=(7.311/(7.311+0.546))*\ 8.35*10^{-7}=7.77*10^{-7}\ cm^3$

$M_{TiO2\text{-}B}=7.77*10^{-7}\ cm^3*3.616g/cm^3=2.81*10^{-6}\ g$

$V_{Pt}=(0.546/(7.311+0.546))*\ 8.35*10^{-7}=5.80*10^{-8}\ cm^3$

$M_{Pt}=5.80*10^{-8}\ cm^3*21.45\ g/cm^3=1.25*10^{-6}\ g$

$M_{total}=M_{TiO2\text{-}B}+M_{Pt}=4.06*10^{-6}\ g$

Thus, it has a theoretical capacity of $4.06*10^{-6}$ g *335mAh/g=1.36×10^{-3} mAh. Since 1C refers to full charge or discharge its capacity in one hour, 1C current equals to 1.36uA for this sample.

The Pt:TiO_2-B thin film with 6% Pt, 33% Ti and 61% O has the weight of $4.405*10^{-6}$g and 1C current of 1.137uA, calculated in the same fashion as above. And the Pt:TiO_2-B thin film with 12% Pt, 30% Ti and 58% O has the weight of $5.20*10^{-6}$g and 1C current of 1.74uA.

(a)

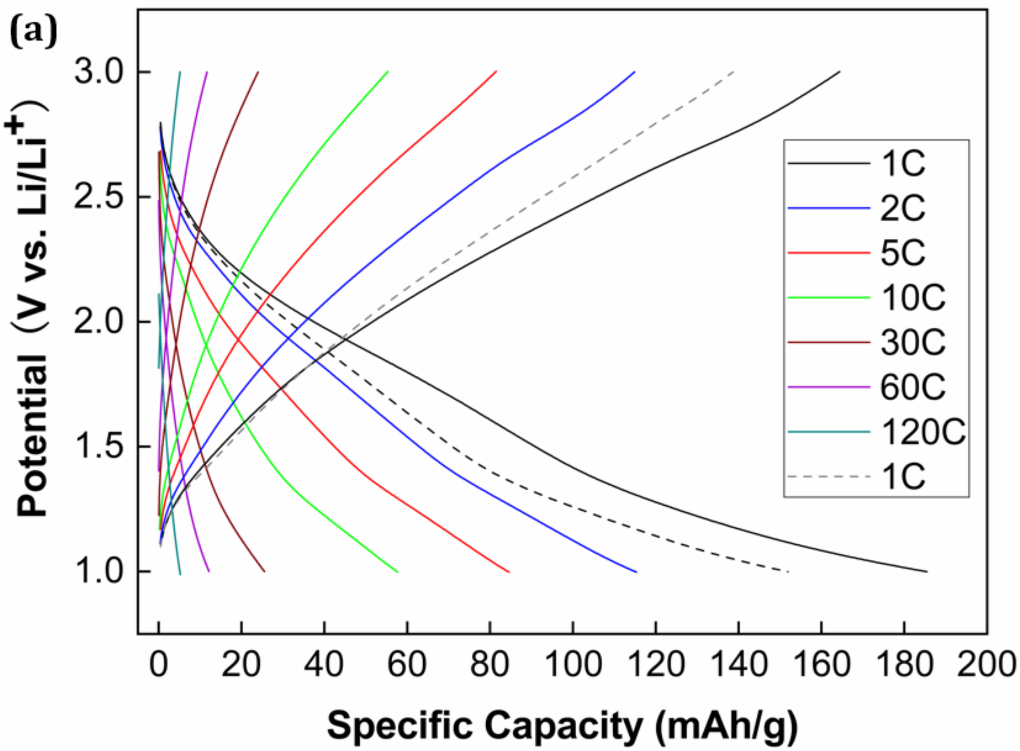

3.0
2.5
2.0
1.5
1.0
Potential (V vs. Li/Li+)
0
20
40
60
80
100
120
140
160
180
200
Specific Capacity (mAh/g)
1C
2C
5C
10C
30C
60C
120C
1C

(b)

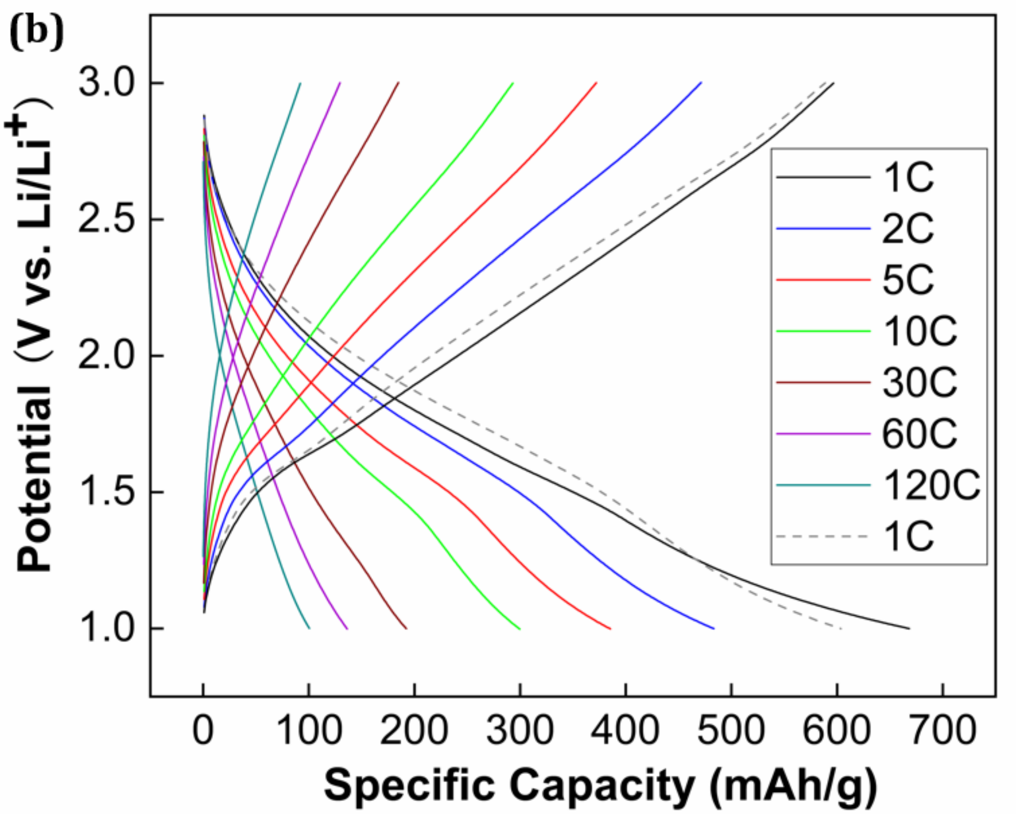

3.0
2.5
2.0
1.5
1.0
Potential (V vs. Li/Li+)
0
100
200
300
400
500
600
700
Specific Capacity (mAh/g)
1C
2C
5C
10C
30C
60C
120C
1C

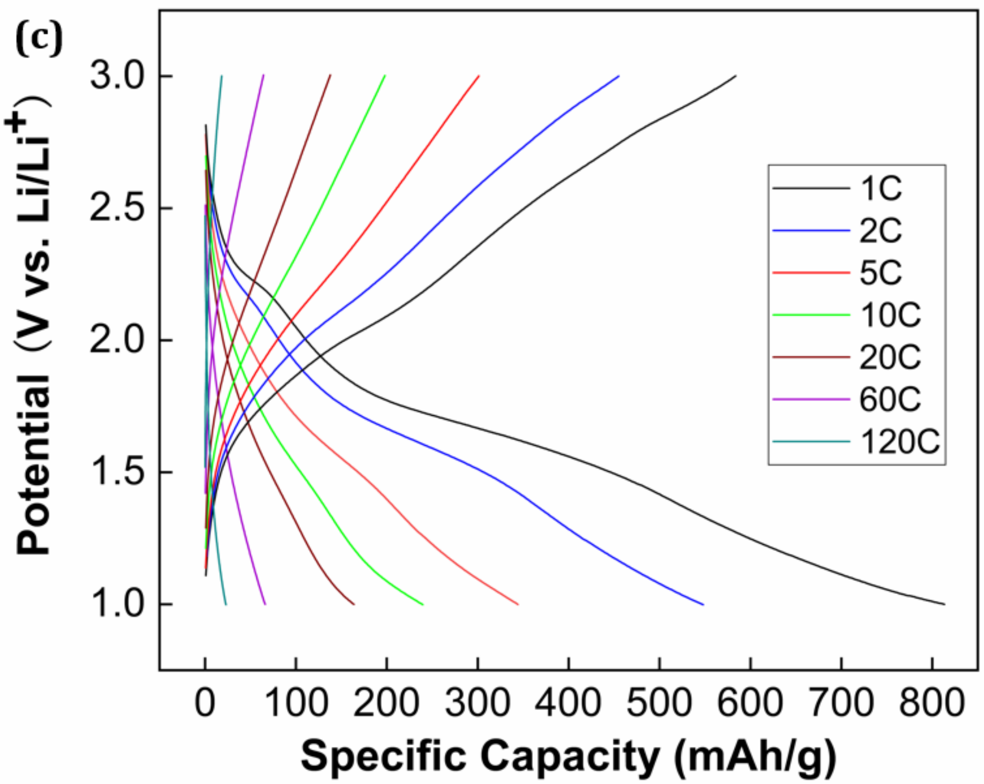
(c)
Potential (V vs. Li/Li+)
Specific Capacity (mAh/g)
1C
2C
5C
10C
20C
60C
120C
3.0
2.5
2.0
1.5
1.0
0
100
200
300
400
500
600
700
800

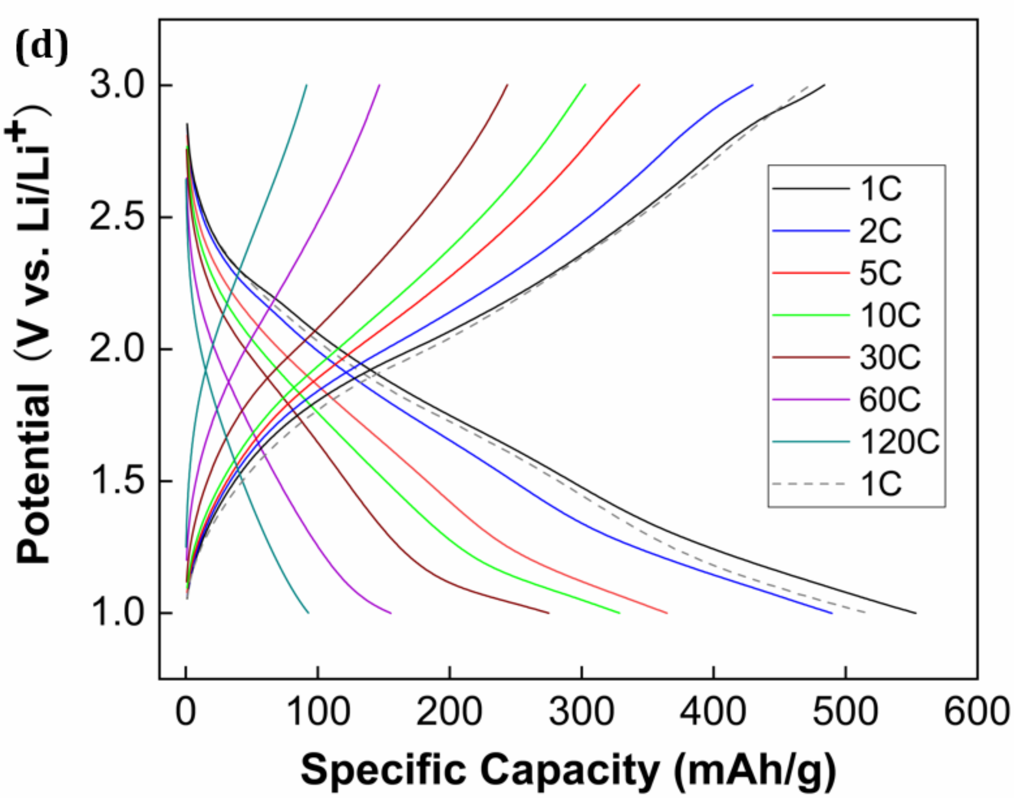
(d)
Potential (V vs. Li/Li+)
Specific Capacity (mAh/g)
1C
2C
5C
10C
30C
60C
120C
1C
3.0
2.5
2.0
1.5
1.0
0
100
200
300
400
500
600

Figure 3.7 Galvanostatic charge-discharge profiles of Ca:TiO_2-B (a) and Pt:TiO_2-B thin films on (100) $SrTiO_3$ substrate with (b) 1.5% (c) 6% (d) 12% Pt content at each current rate from 1C to 120C and then return to 1C.

Figure 3.7 presents the first galvanostatic charge-discharge curves of Ca:TiO_2-B and Pt: TiO_2-B thin film with Pt content of 1.5%, 6% and 12% at each current rate from 1C to 120C and then return to 1C, the largest charge capacity among them can reach over 800 mAh/g for the Pt:TiO_2-B thin film with Pt content of 6% in the first cycle, which doubles the theoretical capacity of TiO_2-B, but the first discharge capacity is only 583.71 mAh/g, so the coulombic efficiency only reaches 70%, signifying a high irreversible capacity in the first cycle. This phenomenon can be ascribed to the formation of solid electrolyte interface (SEI) layer at the surface of the anode material in the first cycle. [55]SEI layer is formed by the reaction between anode materials and electrolyte. Some irreversible capacity is created during this process, which results in the high value of the discharge capacity. The formation of SEI layers has a critical impact on the performance of the electrode material. [56][57][58][59] On the one hand, the formation of SEI film consumes part of the lithium ion, so that the irreversible capacity of the first charge and discharge process is increased, and the charge and discharge efficiency of the electrode material is lowered; On the other hand, the stable SEI layer is insoluble in organic solvents, so that it can be stably present in an organic electrolyte solution, and the solvent molecule cannot pass through the passivation layer, thereby effectively preventing co-intercalation of solvent molecules and avoiding the damage caused by the embedded electrode material, thus greatly improving the cycle performance and lifetime of the electrode.

It is very prominent that Pt:TiO_2-B thin film with different Pt content all have significantly larger specific capacity than pure Ca:TiO_2-B thin film, which indicates that Pt can effectively improve the electrochemical performance of TiO_2-B thin film. One possible explanation to this phenomenon is that Pt can increase the electronic and ionic conductivity in the lithium-ion battery system so that more lithium ions can be transported in and out of anode materials, but detailed mechanism of enhancement still needs to be investigated by in-situ XRD and TEM to deduce the role of Pt played in the charge and discharge process. Another possible reason for such high specific capacity might relates to the double-layer charging, which is a non-Faradic process. [60] When the electrode materials touch the electrolyte, causing the charges to be arranged and allowing Li-ions to be stored near the surface of electrode except for the part that intercalated into the crystal structure. Thus, this double-layer charging process will significantly increase the specific capacity of electrode materials.

With the current increased from 1C to 120C, the specific capacity of all four samples decreased considerably because only a small amount of Pt:TiO_2-B thin film near the electrode surface can actually be lithiated at high current rate. When the current rate was reset back to 1C, both the Pt:TiO_2-B thin films with the Pt content of 1.5% and 12% can still retain high specific capacity of nearly 90%, which shows excellent endurance of this potential anode material. Even though the Pt:TiO_2-B thin film with the Pt content of 6% has high specific capacity up to more 800 mAh/g in 1C current, but its capacity drops much more severe than the other two Pt: TiO_2-B thin films. When the current rate rises to 120C, it only has specific capacity of 18.43 mAh/g, which is not favorable for its application that requires fast charge and discharge capabilities. However, both the Pt:TiO_2-B thin films with the Pt content of 1.5% and 12% can still maintain about 100 mAh/g at 120C current rate, which reveals the superiority of these two materials as anode materials for LIBs.

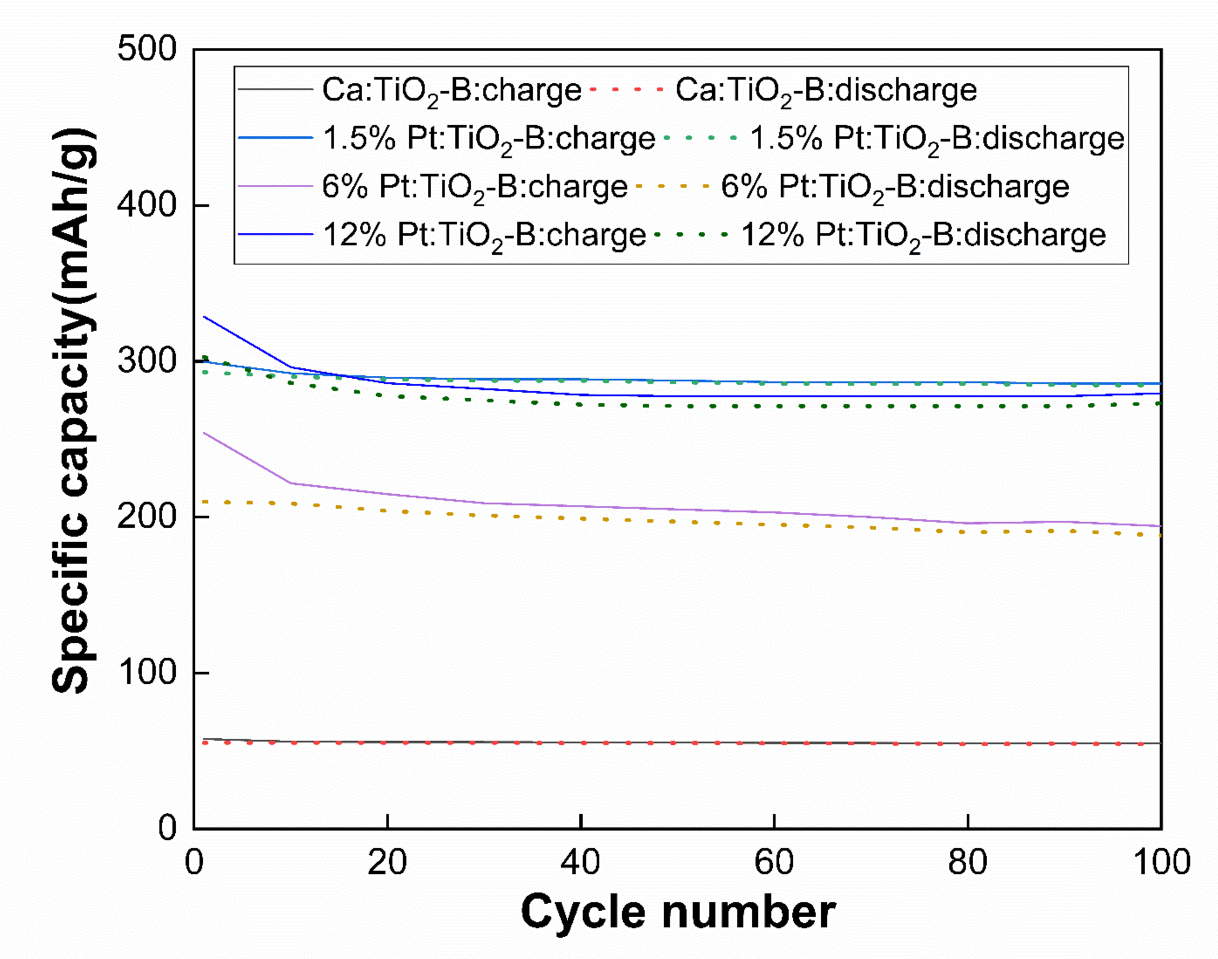

Figure 3.8 Specific capacities of Ca:TiO_2-B and Pt:TiO_2-B thin film on (100) $SrTiO_3$ substrate with 1.5%, 6% and 12% Pt content at a charge-discharge rate of 10C for 100 cycles.

Cycling stability is another important aspect for the evaluation of electrode materials. Therefore, each sample were charged and discharged at the current rate of 10C for 100 cycles to test its cycling stability as shown in Figure 3.8, the specific capacity can still maintain at nearly 300 mAh/g for the Pt:TiO_2-B thin film with Pt content of 1.5% and 12%

in the 100th cycle under 10C current rate, while the specific capacity of Pt:TiO_2-B thin film with Pt content of 6% has decreased to roughly 200 mAh/g and Ca:TiO_2-B possesses much lower specific capacity down to about 55 mAh/g under the same treatment. Thus, Pt:TiO_2-B thin films with 1.5% and 12% Pt content have better electrochemical performance in capacity retention than pure Ca:TiO_2-B and Pt:TiO_2-B thin film with Pt content of 6% under long cycling test. In additional, we can find out that all the potential anode materials maintain high coulombic efficiency of almost 97% in most cycles. The capacity loss and low coulombic efficiency in the first ten cycles is visible in samples of both Ca:TiO_2-B and Pt:TiO_2-B thin film due to their low electronic conductivity. After 10 cycles, however, the capacity loss is much lower than the first 1o cycles and the coulombic efficiency restored to nearly 97% for Ca:TiO_2-B and Pt:TiO_2-B thin film with Pt content of 1.5% and 12%, but the one with Pt content of 6% has relatively lower coulombic efficiency around 95%.

3.6 Cyclic Voltammetry (CV) tests

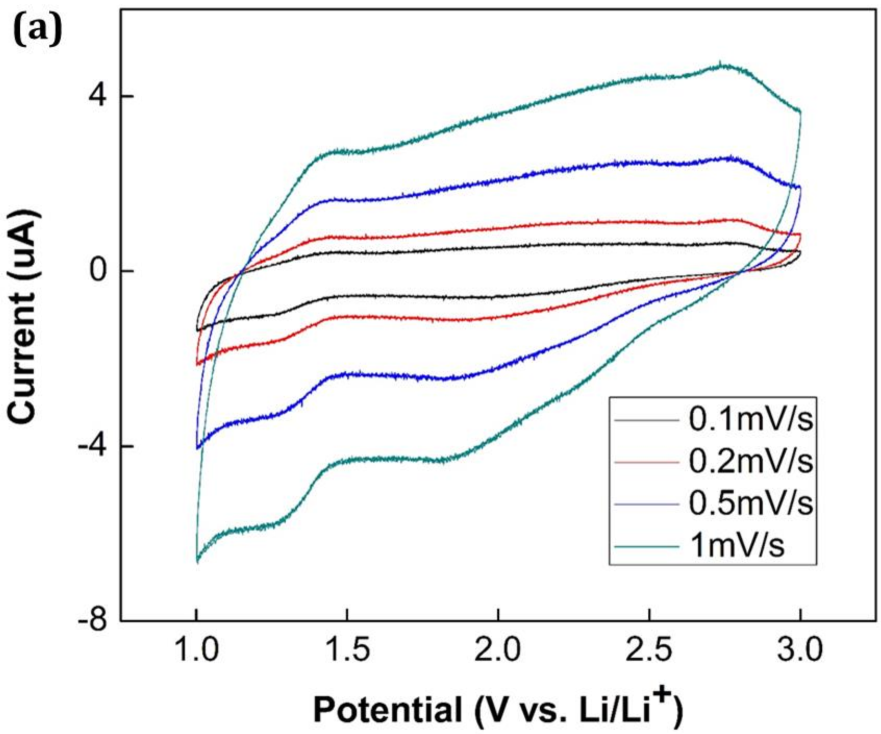

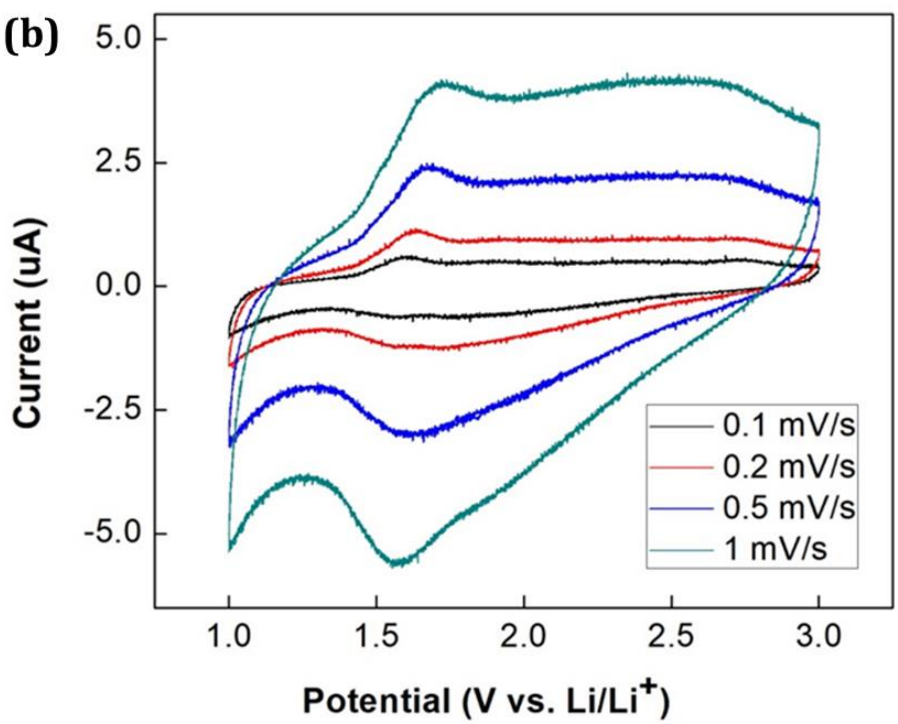

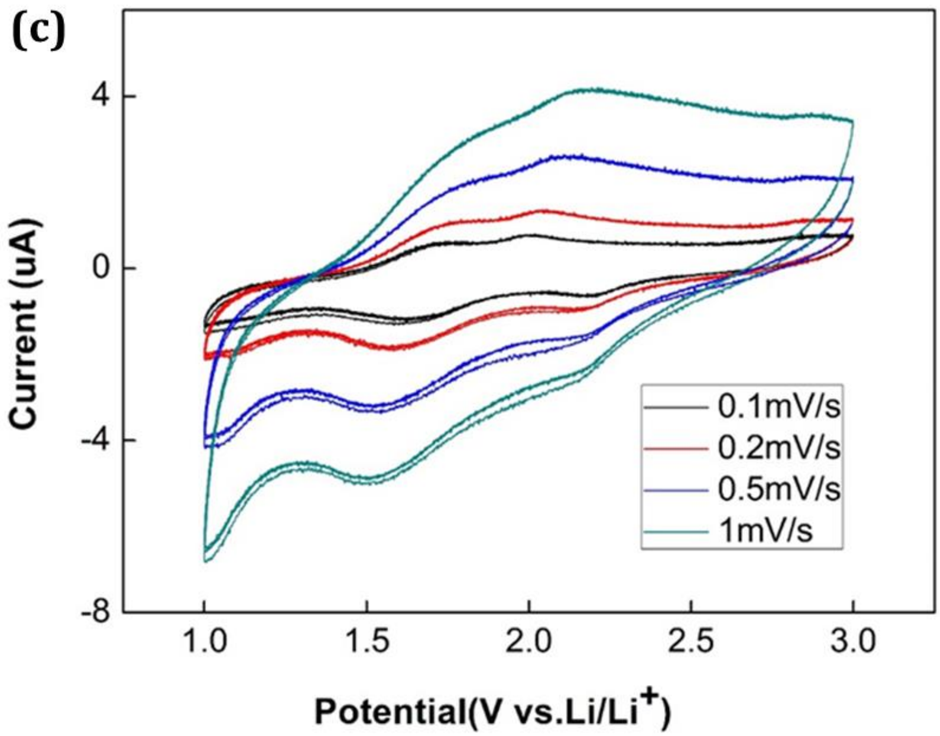
(c)
4
0
-4
-8
1.0
1.5
2.0
2.5
3.0
Current (uA)
Potential(V vs.Li/Li+)
0.1mV/s
0.2mV/s
0.5mV/s
1mV/s

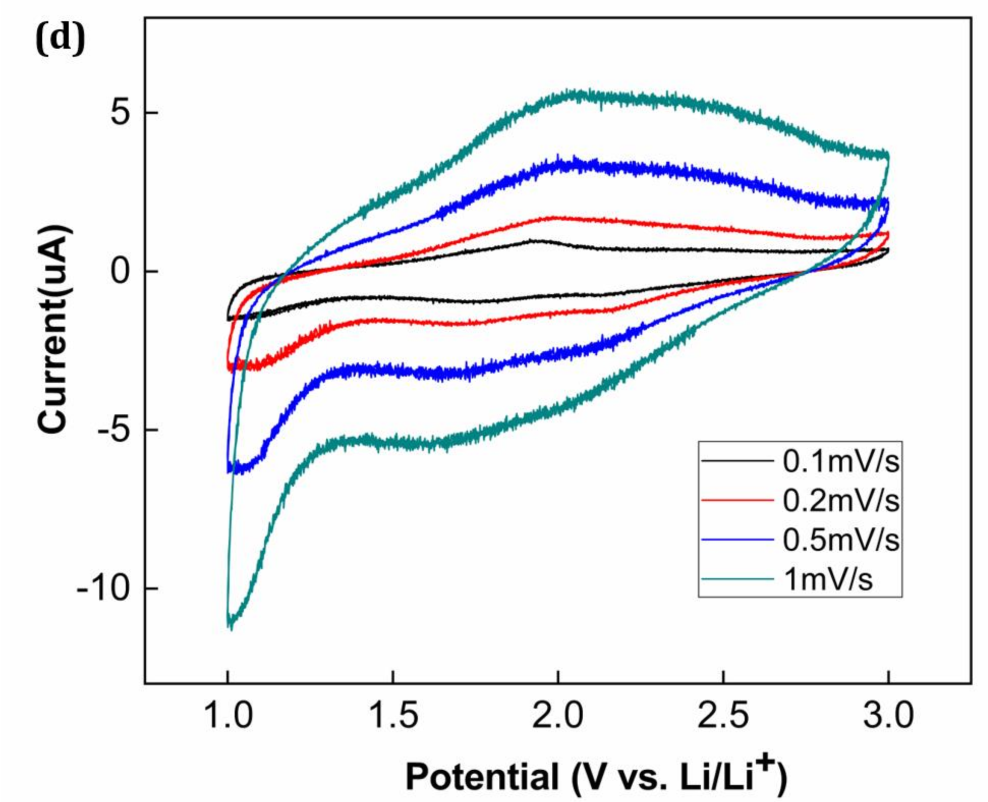
(d)
5
0
-5
-10
1.0
1.5
2.0
2.5
3.0
Current(uA)
Potential (V vs. Li/Li+)
0.1mV/s
0.2mV/s
0.5mV/s
1mV/s

Figure 3.9 Cyclic voltammetry (CV) curves of Ca:TiO_2-B (a) and Pt:TiO_2-B thin film on (100) $SrTiO_3$ substrate with (b) 1.5% (c) 6% (d) 12% Pt content from 1.0V-3.0V at scan rates from 0.1mV/s to 1mV/s.

Lithium ion's intercalation and deintercalation process of the as-prepared anode material are revealed by the cyclic voltammetry (CV) measurement. In the CV graphs in Figure 3.9, we can find that there is an evident peak located at 1.25V, which should also be attributed to the formation of SEI layer at the surface of the anode material[55]. These peaks disappeared after three cycles which indicates that SEI layer can segregate the anode material from electrolyte to prevent further reaction between the electrolyte and anode materials. A pair of redox peaks at roughly 1.5 V and 1.75V can be noticed in the sample with Pt content of 1.5%, which represents the pseudocapacitive Li^+ intercalation and deintercalation process of TiO_2-B, respectively. [27][40] The other two Pt:TiO_2-B samples have redox peaks at roughly 1.5V and 2.0V, which also corresponds to the Li-ion insertion and extraction process in TiO_2 lattice.[55] The specific capacity of each sample calculated by integrating the cyclic voltammograms fit well with the value obtained by chronopotentiometry tests.

CHAPTER 4: Conclusions and Future work

In conclusion, Pt:TiO_2-B thin film was prepared by PLD (pulsed laser deposition) successfully verified by TEM images and is an potential candidate for anode material of LIBs. It is reasonable to conclude that Pt dopant plays an important role in upgrading the TiO_2-B electrochemical performance as anode material of LIBs. Among all the three Pt:TiO_2-B thin films with Pt content of 1.5%, 6% and 12% we prepared, the one with Pt content of 1.5% has the best electrochemical performance up to 668.2 mAh/g in 1C current and still has specific capacity of 603.66 mAh/g after intensive cycling. But the mechanism of enhancement by such a small amount of Pt still needs to be investigated by more advanced techniques, such as in-situ XRD and TEM, since the electronic conductivity is not improved measurably by Hall effect measurement. The Pt:TiO_2-B thin film with Pt content of 12%, whose conductivity has been improved significantly, also shows good electrochemical performance that is comparable to the one with Pt content of 1.5%, which proves our initial hypothesis for this project. The Pt:TiO_2-B thin film Pt content of 6% has relatively poor performance compared with the other two samples, while it is still far superior than pure Ca:TiO_2-B thin film.

Our work provides a candidate high-performance anode material for lithium-ion batteries. Coupled with other high-performance cathode material, such as $LiFePO_4$ and other modifications, [1][38]that can express the entire capacity of Pt:TiO_2-B thin film, these two material will become a promising combination of electrode materials for lithium-ion batteries. In addition, doping conductive substances inside TiO_2 matrix is an effective way to elevate the electrochemical performance of TiO_2-based materials with low electronic and ion conductivity as anode materials. Pulsed laser deposition, a waterless synthesis method, should also be paid more attention considering its advantage over traditional hydrothermal method when preparing high-quality crystalline TiO_2-B thin film. This thesis project would be instructive for the improvement of electrode materials with poor electronic conductivity for lithium ion batteries.

Future work on relative projects should focus on finding proper and effective dopant materials and synthesis procedures for improvement on conductivity and explaining the mechanisms of conductive substances played in the enhancement.

REFERENCE

[1] B. Kang , G. Ceder. Battery materials for ultrafast charging and discharging. Nature, 2009, 458, 190-193.

[2] Goodenough, J. B.; Kim, Y. Challenges for Rechargeable Li Batteries. Chemistry of Materials. 2010, 22, 587–603.

[3] M. S. Whittingham． Electrical Energy Storage and Intercalation Chemistry. Science, 1976, 11, 1126-1127

[4] Armand MB. Intercalation electrodes, Materials for advanced batteries. Springer US. 1980, 145-161．

[5] Mitzushima K, Johnes P C, Wiseman P J, Goodenough J B. $Li_xC_0O_2(0<x<1)$： A new cathode material for bakeries of high energy density. Materials Research Bulletin, 1980, 15, 783-789.

[6] Auborn JJ， Barberio YL. Lithium intercalation cells without metallic lithium MoO2/LiCoO2 and WO2/LiCoO2. Journal of Electrochemical Society. 1987, 134(3), 63 8-641.

[7] Tarascon J M, Armand M. Issues and challenges facing rechargeable lithium batteries. Nature, 2001, 414(6861), 359-367．

[8] Etacheri, Vinodkumar, Yourey, Joseph E., Bartlett, Bart M. Chemically bonded TiO2-Bronze nanosheet/reduced graphene oxide hybrid for high-power lithium ion batteries. ACS Nano, 2014, 8, 1491-1499.

[9] Fergus, Jeffrey W. Recent developments in cathode materials for lithium ion batteries. Journal of Power Sources, 2010, 195, 939-954.

[10] Kalluri, Sujith, Yoon, Moonsu, Jo, Minki, Park, Suhyeon, Myeong, Seungjun, Kim, Junhyeok. Surface Engineering Strategies of Layered LiCoO2 Cathode Material to Realize High-Energy and High-Voltage Li-Ion Cells. Advanced energy materials, 2017, 7, 1-21.

[11] Goriparti S, Miele E, De Angelis F, et a1. Review on recent progress of nanostructured anode materials for Li-ion batteries. Journal of Power Sources. 2014, 257, 421-443.

[12] Xiao, Xingcheng, Liu, Ping, Wang, John S, Verbrugge, M. W, Balogh, Michael P. Vertically aligned graphene electrode for lithium ion battery with high rate capability. Electrochemistry Communications, 2011, 13, 209-212.

[13] Guo, Peng, Song, Huaihe, Chen, Xiaohong. Electrochemical performance of graphene nanosheets as anode material for lithium-ion batteries. Electrochemistry Communications, 2009, 11, 1320-1324.

[14] Charles de las Casas, Wenzhi Li. A review of application of carbon nanotubes for lithium ion battery anode material. Journal of Power Sources. 2012, 208, 74-85.

[15] Natarajan, C. Setoguchi, K. Nogami, G. Preparation of a nanocrystalline titanium dioxide negative electrode for the rechargeable lithium ion battery. Electrochimica Acta, 1998, 43, 3371-3374.

[16] Lafont, U. Carta, D. Mountjoy, G. Chadwick, A. V. Kelder, E. M. In situ structural changes upon electrochemical lithium insertion in nanosized anatase TiO2. Journal of Physical Chemistry C, 2010, 114, 1372-1378.

[17] Dylla, A. G, Lee, J. A, Stevenson, K. J. Influence of Mesoporosity on Lithium-Ion Storage Capacity and Rate Performance of Nanostructured TiO2(B). Langmuir 2012, 28, 2897–2903.

[18] Ren, Y, Liu, Z, Pourpoint, F, Armstrong, A. R, Grey, C. P, Bruce, P. G. Nanoparticulate TiO2(B): An Anode for Lithium-Ion Batteries. Angewandte Chemie - International Edition. 2012, 51, 2164–2167

[19] Van de Krol R, Goossens A, Schoonman J. Spatial extent of lithium intercalation in anatase TiO2. The Journal of Physical Chemistry B, 1999, 103, 7151-7159.

[20] Hu Y S, Kienle L, Guo Y G, et al. High lithium electroactivity of nanometer-sized rutile TiO2. Advanced Materials, 2006, 18, 1421-1426.

[21] Dambournet, Damien, Belharouak, Ilias, Amine, Khalil. Tailored Preparation Methods of TiO2 Anatase, Rutile, Brookite: Mechanism of Formation and Electrochemical Properties. Chemistry of Materials, 2010, 22, 1173-1179

[22] Marchand, René, Brohan, Luc, Tournoux, Michel. TiO2(B) a new form of titanium dioxide and the potassium octatitanate K2Ti8O17. Materials Research Bulletin, 1980, 1129-1133.

[23] Zhenguo Yang, Daiwon Choi, Sebastien Kerisit, Kevin M. Rosso, Donghai Wang, Jason Zhang, Gordon Graff, Jun Liu. Nanostructures and lithium electrochemical reactivity of lithium titanites and titanium oxides: A review. Journal of Power Sources, 2009, 192, 588-598.

[24] L. Kavan, M. Gra1tzel, S. E. Gilbert, C. Klemenz, and H. J. Scheel. Electrochemical and Photoelectrochemical Investigation of Single-Crystal Anatase. J. Am. Chem. Soc. 1996, 118, 6716-6723.

[25] Zhang, Kui, Katz, Michael B., Li, Baihai, Kim, Sung Joo, Du, Xianfeng, Hao, Xiaoguang, Jokisaari, Jacob R. Zhang, Shuyi, Graham, George W. Van Der Ven, Anton, Bartlett, Bart M. Pan, Xiaoqing. Water-free titania-bronze thin films with superfast lithium-ion transport. Advanced Materials, 2014, 26, 7365-7370.

[26] Zukalová, Markéta, Kalbáč, Martin, Kavan, Ladislav, Exnar, Ivan, Graetzel, Michael. Pseudocapacitive lithium storage in TiO2(B). Chemistry of Materials, 2005, 17, 1248-1255.

[27] Augustyn, Veronica, Come, Jérémy, Lowe, Michael A., Kim, Jong Woung, Taberna, Pierre Louis, Tolbert, Sarah H., Abruña, Héctor D., Simon, Patrice, Dunn, Bruce. High-rate electrochemical energy storage through Li + intercalation pseudocapacitance. Nature Materials, 2013, 12, 518-522.

[28] A. Lotnyk , S. Senz , D. Hesse , Thin Solid Films 2007, 515, 3439-3447.

[29] Liu, Hao, Li, Wei, Shen, Dengke, Zhao, Dongyuan, Wang, Guoxiu. Graphitic Carbon Conformal Coating of Mesoporous TiO2 Hollow Spheres for High-Performance Lithium Ion Battery Anodes. Journal of the American Chemical Society, 2015, 137, 13161-13166.

[30] Mo, Runwei, Lei, Zhengyu, Sun, Kening, Rooney, David. Facile synthesis of anatase TiO2 quantum-dot/graphene-nanosheet composites with enhanced electrochemical performance for lithium-ion batteries. Advanced Materials, 2014, 26, 2084-2088.

[31] Chen, Zheng, Zhang, Dieqing, Wang, Xiaolei, Jia, Xilai, Wei, Fei, Li, Hexing, Lu, Yunfeng. High-performance energy-storage architectures from carbon nanotubes and nanocrystal building blocks. Advanced Materials, 2012, 24, 2030-2036.

[32] Zhen M, Guo S, Gao G, et al. TiO2-B nanorods on reduced graphene oxide as anode materials for Li ion batteries. Chemical Communications, 2015, 51, 507-510.

[33] Zhang Q, Li R, Zhang M, et al. TiO2 nanocrystals/graphene hybrids with enhanced Li-ion storage performance. Journal of Energy Chemistry, 2014, 23, 403-410.

[34] Liu, Hao, Li, Wei, Shen, Dengke, Zhao, Dongyuan, Wang, Guoxiu. Graphitic Carbon Conformal Coating of Mesoporous TiO2 Hollow Spheres for High-Performance Lithium Ion Battery Anodes. Journal of the American Chemical Society, 2015,137, 13161-13166.

[35] Wang, John, Polleux, Julien, Lim, James, Dunn, Bruce. Pseudocapacitive Contributions to Electrochemical Energy Storage in TiO2 (Anatase) Nanoparticles. The Journal of Physical Chemistry C, 2007, 111, 14925-14931.

[36] He, Ben Lin, Dong, Bin, Li, Hu Lin. Preparation and electrochemical properties of Ag-modified TiO2 nanotube anode material for lithium-ion battery. Electrochemistry Communications, 2007, 9, 425-430.

[37] Xu, Jinwei, Jia, Caihong, Cao, Bin, Zhang, W. F. Electrochemical properties of anatase TiO2 nanotubes as an anode material for lithium-ion batteries. Electrochimica Acta, 2007, 52, 8044-8047.

[38] Armstrong, G, Armstrong, A. R, Bruce, P. G, Reale, P, Scrosati, B. TiO2(B) Nanowires as an Improved Anode Material for Lithium-Ion Batteries Containing LiFePO4 or LiNi0.5Mn1.5O4 Cathodes and a Polymer Electrolyte. Advanced Materials, 2006, 28, 2597-2600

[39] Li, Wei, Wang, Fei, Feng, Shanshan, Wang, Jinxiu, Sun, Zhenkun, Li, Bin, Li, Yuhui, Yang, Jianping, Elzatahry, Ahmed A, Xia, Yongyao, Zhao, Dongyuan. Sol-gel design strategy for ultradispersed tio2 nanoparticles on graphene for high-performance lithium ion batteries. Journal of the American Chemical Society. 2013, 135, 18300-18303.

[40] Liu, Shaohua, Jia, Haiping, Han, Lu, Wang, Jiulin, Gao, Pengfei, Xu, Dongdong, Yang, Jun, Che, Shunai. Nanosheet-constructed porous TiO2-B for advanced lithium ion batteries. Advanced Materials. 2012, 24, 3201-3204.

[41] Kim, Sung Joo, Lei, Pei, Zhang, Kui, Zhou, Chang, Graham, George W., Pan, Xiaoqing. Tunable, Endotaxial Inclusion of Crystalline Pt-Based Nanoparticles Inside a High-Quality Bronze TiO2 Matrix. Chemistry of Materials, 2017, 29, 2016-2023

[42] Armstrong, A. Robert, Armstrong, Graham, Canales, Jesús, García, Raquel, Bruce, Peter G. Lithium-ion intercalation into TiO2-B nanowires. Advanced Materials, 2005, 17, 862-865.

[43] Armstrong, Graham, Armstrong, A. Robert, Canales, Jesús, Bruce, Peter G. Nanotubes with the TiO2-B structure. Chemical Communications, 19, 2454-2456.

[44] Beuvier, Thomas, Richard-Plouet, Mireille, Mancini-Le Granvalet, Maryline, Brousse, Thierry, Crosnier, Olivier, Brohan, Luc. TiO2(B) nanoribbons as negative electrode material for lithium ion batteries with high rate performance. Inorganic Chemistry, 2010, 49, 8457-8464.

[45] Liu, Hansan, Bi, Zhonghe, Sun, Xiao Guang, Unocic, Raymond R., Paranthaman, M. Parans, Dai, Sheng, Brown, Gilbert M. Mesoporous TiO2-B microspheres with superior rate performance for lithium ion batteries. Advanced Materials, 2011, 23, 3450-3454.

[46] Kogure, Toshihiro, Umezawa, Taku. Formation of TiO2 (B) Nanocrystallites in Sol-Gel-Derived SiO2-TiO2 Film. Journal of the American Ceramic Society, 1999, 50, 3248-3250.

[47] Zhou, Weijia, Gai, Ligang, Hu, Peiguang, Cui, Jingjie, Liu, Xiaoyan, Wang, Dongzhou, Li, Guohong, Jiang, Huaidong, Liu, Duo, Liu, Hong, Wang, Jiyang. Phase transformation of

TiO2 nanobelts and TiO 2(B)/anatase interface heterostructure nanobelts with enhanced photocatalytic activity. CrystEngComm, 2011, 13, 6643-6649.

[48] Etacheri, Vinodkumar, Kuo, Yenting, Van Der Ven, Anton, Bartlett, Bart M. Mesoporous TiO2-B microflowers composed of (1 1 0) facet-exposed nanosheets for fast reversible lithium-ion storage. Journal of Materials Chemistry A, 2013, 1, 12028-12032.

[49] Van der Pauw, L. J. Philips Res. Repts. 1958, 13, 1

[50] Kim, Y. J.; Jin, S. B.; Kim, S. I.; Choi, Y. S.; Choi, I. S.; Han, J. G. Effect of oxygen flow rate on ITO thin films deposited by facing targets sputtering. Thin Solid Films 2010, 518, 6241−6244.

[51] Park, S.-J.; Lee, J.-P.; Jang, J. S.; Rhu, H.; Yu, H.; You, B. Y.; Kim, C. S.; Kim, K. J.; Cho, Y. J.; Baik, S.; Lee, W. In situ control of oxygen vacancies in TiO2 by atomic layer deposition for resistive switching devices. Nanotechnology 2013, 24, 295202.

[52] Zhang, L.; Ge, S.; Zuo, Y.; Zhang, B.; Xi, L. Influence of Oxygen Flow Rate on the Morphology and Magnetism of SnO2 Nanostructures. J. Phys. Chem. C 2010, 114, 7541−7547

[53] Pan, X.; Xu, Y.-J. Defect-Mediated Growth of Noble-Metal (Ag, Pt, and Pd) Nanoparticles on TiO2 with Oxygen Vacancies for Photocatalytic Redox Reactions under Visible Light. J. Phys. Chem. C 2013, 117, 17996−18005.

[54] Chang, T.-Y.; Tanaka, Y.; Ishikawa, R.; Toyoura, K.; Matsunaga, K.; Ikuhara, Y.; Shibata, N. Direct Imaging of Pt Single Atoms Adsorbed on TiO2 (110) Surfaces. Nano Lett. 2014, 14, 134−138

[55] Qiu, Jingxia, Zhang, Peng, Ling, Min, Li, Sheng, Liu, Porun, Zhao, Huijun, Zhang, Shanqing. Photocatalytic Synthesis of TiO_2 and Reduced Graphene Oxide Nanocomposite for Lithium Ion Battery. ACS Applied Materials & Interfaces, 2012, 4, 3636-3642

[56] Verma, Pallav, Maire, Pascal, Novák, Petr. A review of the features and analyses of the solid electrolyte interphase in Li-ion batteries. Electrochimica Acta, 2010, 55, 6332-6341

[57] He, Ben Lin, Dong, Bin, Li, Hu Lin. Preparation and electrochemical properties of Ag-modified TiO2nanotube anode material for lithium-ion battery. Electrochemistry Communications, 2007, 9, 425-430.

[58] Brutti, Sergio, Gentili, Valentina, Menard, Hervé, Scrosati, Bruno, Bruce, Peter G. TiO2-(B) nanotubes as anodes for lithium batteries: Origin and mitigation of irreversible capacity. Advanced Energy Materials, 2012, 2, 322-327.

[59] Wang, Yong Qing, Gu, Lin, Guo, Yu Guo, Li, Hong, He, Xiao Qing, Tsukimoto, Susumu, Ikuhara, Yuichi, Wan, Li Jun. Rutile-TiO2nanocoating for a high-rate Li4Ti5O12anode of a lithium-ion battery. Journal of the American Chemical Society, 2012, 134, 7874-7879.

[60] Jha, Gaurav, Tran, Thien, Qiao, Shaopeng, Ziegler, Joshua M, Ogata, Alana F, Dai, Sheng, Xu, Mingjie, Thai, Mya Le, Chandran, Girija Thesma, Pan, Xiaoqing, Penner, Reginald M. Electrophoretic Deposition of Mesoporous Niobium(V)Oxide Nanoscopic Films. Chemistry of Materials. 2018, 30, 6549-6558.